The Plant Cell, Vol. 32: 3170–3187, October 2020, www.plantcell.org © 2020 ASPB.

The Tip-Localized Phosphatidylserine Established by Arabidopsis ALA3 Is Crucial for Rab GTPase-Mediated Vesicle Trafficking and Pollen Tube Growth[OPEN]

Yuelong Zhou,[a,1] Yang Yang,[a,1] Yue Niu,[a,1] TingTing Fan,[a] Dong Qian,[a] Changxin Luo,[a] Yumei Shi,[a] Shanwei Li,[b] Lizhe An,[a] and Yun Xiang[a,2]

[a] MOE Key Laboratory of Cell Activities and Stress Adaptations, School of Life Sciences, Lanzhou University, Lanzhou 730000, China
[b] State Key Laboratory of Crop Biology, College of Life Sciences, Shandong Agricultural University, Tai'an 271018, China

RabA4 subfamily proteins, the key regulators of intracellular transport, are vital for tip growth of plant polar cells, but their unique distribution in the apical zone and role in vesicle targeting and trafficking in the tips remain poorly understood. Here, we found that loss of Arabidopsis (*Arabidopsis thaliana*) AMINOPHOSPHOLIPID ATPASE 3 (ALA3) function resulted in a marked decrease in YFP-RabA4b/ RFP-RabA4d- and FM4-64-labeled vesicles from the inverted-cone zone of the pollen tube tip, misdistribution of certain intramembrane compartment markers, and an obvious increase in pollen tube width. Additionally, we revealed that phosphatidylserine (PS) was abundant in the inverted-cone zone of the apical pollen tube in wild-type Arabidopsis and was mainly colocalized with the trans-Golgi network/early endosome, certain post-Golgi compartments, and the plasma membrane. Loss of ALA3 function resulted in loss of polar localization of apical PS and significantly decreased PS distribution, suggesting that ALA3 is a key regulator for establishing and maintaining the polar localization of apical PS in pollen tubes. We further demonstrated that certain Rab GTPases colocalized with PS in vivo and bound to PS in vitro. Moreover, ALA3 and RabA4d collectively regulated pollen tube growth genetically. Thus, we propose that the tip-localized PS established by ALA3 is crucial for Rab GTPase-mediated vesicle targeting/trafficking and polar growth of pollen tubes in Arabidopsis.

INTRODUCTION

Pollen tube growth is an indispensable event during double fertilization in flowering plants. This peculiar polarized cell growth, in which the elongation occurs only at the tip area and the growth rate is exceedingly high, is distinct from that of most other plant cells. Notably, rapid tip growth requires intracellular transport machinery to continuously deliver essential cargoes to a defined growth site, and this complex process is governed precisely (Hepler et al., 2001; Cheung and Wu, 2008; Johnson et al., 2019). Indeed, there are mainly two kinds of crucial material transport patterns during tip growth: cytoplasmic streaming in the shank region and polarized vesicle trafficking at the apical area of the pollen tube (Hepler et al., 2001; Cheung and Wu, 2008; Chebli et al., 2013). In angiosperms, vesicles with different diameters aggregate into an inverted-cone zone at the apical area of the pollen tube, where large organelles such as endoplasmic reticulum (ER) and Golgi are absent (Cheung and Wu, 2008; Chebli et al., 2013). Because cytoplasmic streaming cannot reach the apical area of the pollen tube, tip-polarized vesicle trafficking is indispensable. Numerous studies have also shown that many cellular activities, including secretion, endocytosis, vesicle recycling, and degradation, play influential and distinct roles in tip growth (Hepler et al., 2001; Zhang et al., 2010; Grebnev et al., 2017). Unfortunately, the precise regulatory mechanism of tip-polarized vesicle trafficking remains unclear.

Rab GTPases are a key class of conserved proteins responsible for vesicle trafficking in eukaryotes, participating in a variety of endomembrane trafficking processes: vesicle budding, transportation, tethering, and membrane fusion (Zerial and McBride, 2001; Stenmark, 2009; Bhuin and Roy, 2014). In Arabidopsis (*Arabidopsis thaliana*), 57 members of Rab GTPases are divided into eight functional subfamilies (named AtRabA to AtRabH; Rutherford and Moore, 2002; Vernoud et al., 2003). Several members of plant Rab GTPases participate in growth and development as well as biotic and abiotic stress responses via vesicle-mediated endomembrane trafficking pathways (Mazel et al., 2004; Woollard and Moore, 2008; Bottanelli et al., 2011; Ebine et al., 2014; Ellinger et al., 2014; Uemura and Ueda, 2014; Yin et al., 2017). Additional evidence of the relationship between Rab GTPases and pollen development and polarized pollen tube growth has been obtained from research on Arabidopsis RabA and RabD (Szumlanski and Nielsen, 2009; Peng et al., 2011). For instance, an Arabidopsis Rab family member, RabA4d, which is homologous to the mammalian Rab11 subfamily, is typically localized at the inverted-cone zone of the pollen tube and is responsible for targeted polar transport of vesicles; additionally, a lack of RabA4d activity leads to severe defects in the polarized growth phenotype of pollen tubes, such as slow growth and increased width of pollen tubes as well as swelling of pollen tubes; RabA4d also participates in the transport of the cell wall and membrane components required for pollen tube growth (Szumlanski and Nielsen, 2009). RabA4b, another member of this subfamily, localizes to the root hair tip (which also exhibits

[1] These authors contributed equally to this work.
[2] Address correspondence to xiangy@lzu.edu.cn.
The authors responsible for distribution of materials integral to the findings presented in this article in accordance with the policy described in the Instructions for Author (www.plantcell.org) is: Yun Xiang (xiangy@lzu.edu.cn).
[OPEN]Articles can be viewed without a subscription.
www.plantcell.org/cgi/doi/10.1105/tpc.19.00844

IN A NUTSHELL

Background: Pollen tube growth is an indispensable event during double fertilization in flowering plants. This peculiar polarized cell growth, in which the elongation occurs only at the tip area and the growth rate is exceedingly high, is distinct from that of most other plant cells. Importantly, the rapid tip growth requires intracellular transport machinery to continuously deliver essential cargoes to the apical growth site. There are two main kinds of crucial material transport patterns during tip growth: cytoplasmic streaming in the shank region and polarized vesicle trafficking at the apical area of the pollen tube. Because cytoplasmic streaming cannot reach the apical area of the pollen tube, tip-polarized vesicle trafficking is indispensable. In angiosperms, many vesicles with different diameters aggregate into an inverted-cone zone at the apical area of the pollen tube. However, the precise regulatory mechanism of tip-polarized vesicle trafficking remains unclear.

Question: What are the subcellular localization and biological function of phosphatidylserine (PS) in Arabidopsis pollen tubes?

Findings: Loss of Arabidopsis AMINOPHOSPHOLIPID ATPASE 3 (ALA3) function resulted in a marked decrease in YFP-RabA4b/ RFP-RabA4d- and FM4-64-labeled vesicles from the inverted-cone zone of the pollen tube tip, misdistribution of the certain intramembrane compartment markers and an obvious increase in pollen tube width. Additionally, PS was abundant in the inverted-cone zone of the apical pollen tube in Arabidopsis and mainly colocalized with markers for the trans-Golgi network/early endosome, certain post-Golgi compartments, and the plasma membrane. Loss of ALA3 function resulted in loss of polar localization of apical PS and significantly decreased PS distribution. We further demonstrated that certain Rab GTPases could colocalize with PS in vivo and bind to PS in vitro. Moreover, ALA3 and RabA4d collectively regulated pollen tube growth genetically. Thus, we propose that the tip localization of PS established by ALA3 is crucial for Rab GTPase-mediated vesicle targeting/trafficking and polar growth of pollen tubes in Arabidopsis.

Next steps: Because Rab GTPases can bind a variety of negatively charged phospholipids in vitro, we wish to know the precise mechanism and function of the interaction between Rab GTPases and different phospholipids.

polarized cell growth) and is widely used to label vesicles at the pollen tube tip (Preuss et al., 2004; Zhang et al., 2010). Similarly, alteration in tobacco Rab11b function also results in abnormal pollen tube growth, suggesting that the role of the RabA4 subfamily in vesicle trafficking is important for polarized growth in plants (de Graaf et al., 2005). However, little is known regarding the detailed regulatory mechanisms that establish and maintain the inverted-cone distribution of RabA4 in pollen tubes or root hairs.

In eukaryotic cells, anionic phospholipids, including phosphatidylinositol phosphates (PIPs), phosphatidylserine (PS), and phosphatidic acid (PA), are among the minor lipids in biomembranes (Caillaud, 2019). In addition to being components of the membrane, anionic phospholipids act as key signaling molecules. For example, the contribution of these lipids to the surface charge, curvature, and lipid packing of the membrane can effectively control the localization and activity of Rab GTPases (Bigay and Antonny, 2012; Simon et al., 2016; Kulakowski et al., 2018). Among these phospholipids, phosphatidylinositol-4-phosphate (PI4P), phosphatidylinositol-4,5-phosphate, and PA are three well-studied anionic lipids that localize to the plasma membrane (PM) of pollen tubes (Kost et al., 1999; Zhao et al., 2010; Potocký et al., 2014; Hempel et al., 2017; Noack and Jaillais, 2017), but another lipid, PS, is mainly enriched in the inverted-cone zone of the tobacco (*Nicotiana tabacum*) pollen tube apex (Platre et al., 2018), suggesting that PS might be involved in vesicle trafficking in the apical area of pollen tubes. The asymmetric distribution of PS contributes to the biological function of this lipid and relies on P4-type ATPases (P_4-ATPases), which flip phosphatidylcholine (PC), phosphatidylethanolamine (PE), and PS across the biomembrane from the extracellular/luminal leaflet to the cytosolic leaflet powered by ATP hydrolysis in eukaryotes (Roland and Graham, 2016). The Arabidopsis P_4-ATPase family consists of 12 members, termed aminophospholipid ATPases 1-12 (ALA1-ALA12). In recent years, progress in the research on flippases in plants has shown that P_4-ATPases have pleiotropic effects on physiological functions, including plant growth and development, reproduction, and adaptation to biotic and abiotic stress (Gomès et al., 2000; Poulsen et al., 2008; Zhang and Oppenheimer, 2009; McDowell et al., 2013; Poulsen et al., 2015; Botella et al., 2016; Guo et al., 2017; Niu et al., 2017; Underwood et al., 2017; Zhang et al., 2020). However, whether ALAs are involved in the establishment of the asymmetric distribution of PS in pollen tubes remains unclear. Further research is also required to clarify the subcellular localization and biological function of PS in pollen tubes.

To better understand the mechanisms of the inverted-cone distribution of apical vesicles and the biological functions of PS in pollen tube tips, we screened Arabidopsis ALA mutants with abnormal distributions of apical vesicles and Rab GTPases as well as PS in pollen tubes. Further, we explored the physiological function of PS in the polar growth of pollen tubes. The findings of this study indicate that PS in the apical area of pollen tubes might function as a phospholipid signaling molecule, regulating the distribution of certain Rab GTPases as well as pollen tube growth.

RESULTS

Mutation in ALA3 Affects the Polarized Distribution of Apical Vesicles and Pollen Tube Width

Bioinformatics analysis shows that six Arabidopsis *ALA* members are abundantly expressed in pollen, including *ALA1*, *ALA3*, *ALA6*,

ALA7, *ALA9*, and *ALA12* (Supplemental Figure 1A). To determine whether and how the ALA family participates in the polarized transport of vesicles at the apical region of pollen tube, we used the lipophilic dye FM4-64 to label the pollen tubes of pollen-expressed ALA mutants and then identified the mutants with abnormal tip-polarized vesicles. In wild-type pollen tubes, FM4-64-labeled vesicles were abundantly located at the inverted-cone zone of the pollen tube (Figure 1A), which was consistent with the previous studies (Szumlanski and Nielsen, 2009; Zhang et al., 2010). Interestingly, we only observed obviously decreased accumulation of vesicles in the inverted-cone zone at the apical region of pollen tube in the *ala3* mutant; the intensity of the fluorescence signal within the apical and shank regions of the pollen tube also decreased but was especially high in the subapical region of the *ala3* pollen tube (Figures 1A and 1B; Supplemental Figures 1B to 1G).

We used RabA4b (a RabA4 subfamily member expressed in vegetative organs and widely used to label tip vesicles in pollen tubes) to verify whether ALA3 affected the localization of RabA4 GTPases (Zhang et al., 2010). As expected, the distribution of YFP-RabA4b-labeled vesicles in *ala3* was consistent with the above results (Figures 1C to 1E). Based on time-lapse imaging analysis of the movement of vesicles in living wild-type and *ala3* pollen tubes, FM4-64- and YFP-RabA4b-labeled vesicles in wild-type pollen tubes could move rapidly through an inverted-cone zone at the tip of the pollen tube (see Supplemental Movies 1 and 2), but the vesicles in the *ala3* pollen tube were scarcely enriched in the apical area, unlike those in the wild type and moved only in a disordered manner between two flanks of the subapical region (see Supplemental Movies 3 and 4). In addition, although the cytoplasmic streaming in the shank region of the pollen tube of *ala3* was not notably changed, the velocity of the vesicles in the apical and subapical regions decreased observably (Figures 1F to 1H). Previous studies have reported that the pollen tube growth rate was decreased in *ala3* (Zhang and Oppenheimer, 2009; McDowell et al., 2013), and we also demonstrated that the pollen tube growth of *ala3* was obviously slower than that of wild-type in vitro (Figures 1I and 1J) and in vivo (Supplemental Figures 2C and 2D). In addition, we found a significant increase in pollen tube width in *ala3* (8.26 $\pm$ 0.96 μm), which was in contrast to the wild-type plants (6.95 $\pm$ 0.83 μm; Figures 1I and 1J), thereby revealing that ALA3 might also be involved in the formation and maintenance of the polar growth of pollen tubes.

To ascertain the relationship between the above phenotypes and the lipid-flipping activity of ALA3, a complementation experiment was performed in an *ala3* mutant, in which the full-length cDNAs of *ALA3* and *ALA3* with a point mutation in the conserved functional site of the *ALA* family, named D413N, were used. We found that only full-length *ALA3* cDNA could rescue the abnormal phenotypes of *ala3* related to the growth and width of pollen tubes (Figures 1I and 1J; Supplemental Figures 2A to 2D), suggesting that loss of function of ALA3 probably led to the above phenotypes and that the lipid flipping activity of ALA3 played a crucial role in determining the growth rate and width of pollen tubes. Moreover, brefeldin A (BFA, a vesicle trafficking inhibitor), wortmannin (Wort, a PI3K inhibitor), and latrunculin B (LatB, an actin depolymerization drug) are widely used to inhibit the polarized tip growth of pollen tubes (Gibbon et al., 1999; Zhang et al., 2010). Treatment of *ala3* and wild-type pollens with the above inhibitors resulted in a decrease in pollen tube growth; however, compared to wild type, the negative effect of BFA on pollen tube length significantly decreased in *ala3* (Figure 1K; Supplemental Figure 2E), whereas both Wort and LatB showed no obvious differences (Supplemental Figures 2F to 2I). Together, our results suggested that loss of function of ALA3 induced the disordered distribution of vesicles and the altered trajectory of vesicular trafficking at the pollen tube tip, which ultimately caused an increase in pollen tube width and defective polar growth of the pollen tube.

ALA3 Is Abundant in the Apical Region of Pollen Tube and Colocalizes with Certain Endomembrane Compartments

Next, the distribution patterns of ALA3 in tissues and organelles were determined. *ALA3* could be abundantly expressed in mature pollen and pollen tubes (Supplemental Figure 3). Using an ALA3-GFP transgenic plant, in which the defective phenotype of *ala3* was almost completely complemented, we found that GFP signals were largely distributed in the apical and subapical regions of the pollen tube and dotted at the tip and shank regions of the pollen tube (Figure 2A). Then, based on time-lapse imaging analysis, the ALA3-GFP moved into the inverted-cone zone at the apical region of the pollen tube and was present in the cytoplasmic streaming in the shank region of the pollen tube (see Supplemental Movie 5). Importantly, ALA3-GFP colocalized with FM4-64 in the apical and shank regions of the pollen tube, suggesting that ALA3 was distributed in both vesicles and PM (Figures 2B to 2D). Furthermore, the colocalization between ALA3-GFP and various organelle markers was identified and quantified, showing that ALA3 chiefly colocalized with markers of the trans-Golgi network (TGN)/early endosome (EE; Pearson correlation coefficient [r_p] was 0.05 and 0.43 in the tip and the shank, respectively), post-Golgi (r_p was 0.55 and 0.43 in the tip and the shank, respectively), and RE (r_p was 0.29 and 0.53 in the tip and the shank, respectively), but not the Golgi (r_p was 0.08 and 0.08 in the tip and the shank, respectively) and late endosome (LE; r_p was 0.10 and 0.11 in the tip and the shank, respectively; Figures 2E to 2J). Kymograph analysis showed the localization of spots in the two channels over time (Figures 2K to 2M; Supplemental Figure 4). In addition, the treatment of ALA3-GFP transgenic plants with endomembrane inhibitors (including BFA, Wort, and LatB) resulted in a significant decrease of the polarized distribution of ALA3-GFP at the pollen tube tip (Supplemental Figure 5), indicating that the tip-polarized localization of ALA3 itself might also rely on polarized tip membrane trafficking.

ALA3 and RabA4d Genetically Regulate the Polar Growth of Pollen Tubes

There are four members of the RabA4 protein subfamily, but only RabA4d can be specifically expressed in pollen tubes (Preuss et al., 2004; Szumlanski and Nielsen, 2009). It has been also reported that RabA4d is located at the inverted-cone zone of the pollen tube and is responsible for targeted polar transport of the TGN/EE-derived secretory vesicles (Szumlanski and Nielsen, 2009). We found that RFP-RabA4d and ALA3-GFP exhibited a similar distribution pattern and colocalized in pollen tube tip in

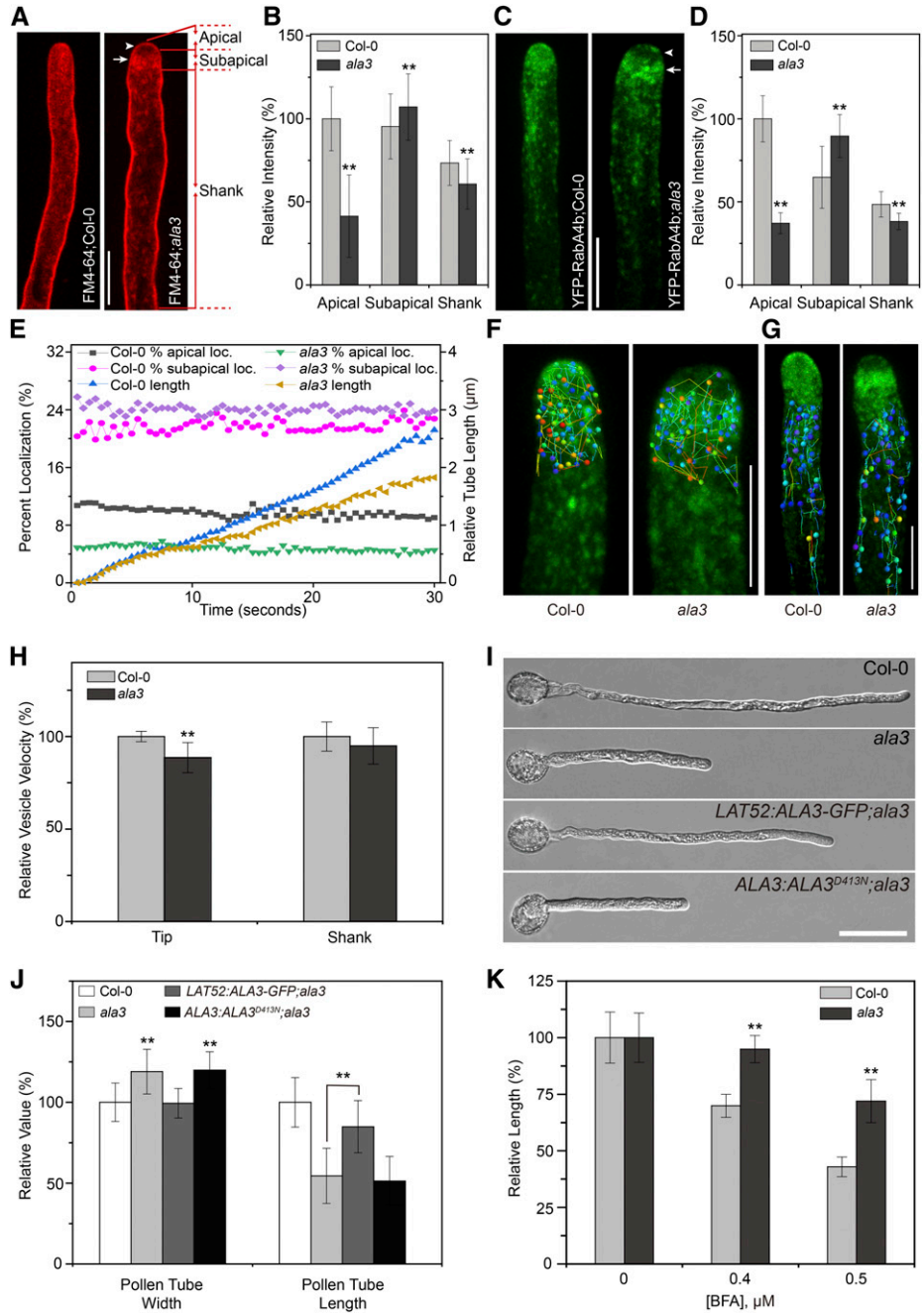

Figure 1. The Distribution Pattern and the Velocity of Apical Vesicles, As Well As the Width of the Pollen Tube, Are Altered in the *ala3* Mutant.

(A) Visualization of the FM4-64 distribution in the pollen tubes from the wild type (Col-0) and *ala3*. Confocal images captured after FM4-64 staining for 20 min. Bar = 10 μm. The arrowhead and arrow indicate the apical and subapical zones, respectively. The apical, subapical, and shank regions used for fluorescence intensity measurement in here and the following pollen tubes are shown on the right.

(B) Quantitative analysis of the relative fluorescence intensity of FM4-64 in the apical, subapical, and shank zones of the pollen tube. The results represent the means ± SDS (n = 30). **P < 0.01 (t test compared to the wild-type values).

(C) Representative confocal images of growing pollen tubes from Col-0 and *ala3* expressing YFP-RabA4b from the same transgenic line. Bar = 10 μm. The arrowhead and arrow indicate the apical and subapical zones, respectively.

(D) Quantitative analysis of the relative fluorescence intensity of YFP-RabA4b in the apical, subapical, and shank zones of the pollen tube. The results represent the means ± SDS (n = 30). **P < 0.01 (t test compared to wild-type values).

certain extent (r_p = 0.52; Figures 3A and 3B). In addition, ALA3-GFP partially colocalized with RFP-RabA4b at the pollen tube tip (r_p = 0.50; Supplemental Figure 6). Moreover, in *ala3*, vesicles labeled with RFP-RabA4d were also mislocalized, which is similar to the result obtained for YFP-RabA4b (Figures 3C to 3E; see Supplemental Movies 6 and 7), indicating that the polar growth of the pollen tube of *ala3* might be directly associated with RabA4d. To further assess whether there is a genetic correlation between ALA3 and RabA4d, the width and length of the pollen tube of the double mutant *ala3 raba4d* were determined. The results showed that the pollen tube of the double mutant *ala3 raba4d* had a similar width as that of the single mutant *raba4d* (Figures 3F to 3H), suggesting that these two genes may work in the same genetic pathway in the regulation of the pollen tube width and polar growth. Next, we also identified the vesicle distribution in *raba4d* labeled with FM4-64. The abundance of apical vesicles labeled with FM4-64 visibly decreased in the *raba4d* pollen tube, and this reduction was directly related to the swelling degree of the pollen tube tip; the more swollen pollen tube tips the fewer apical vesicles (Figures 3I and 3J). This finding showed that loss of function of RabA4d caused anomalies in vesicle distribution in the apical region and polar growth of pollen tubes. In summary, ALA3 might regulate the polar growth of pollen tubes by affecting the function of RABA4d, which in turn controls the vesicle distribution in the inverted-cone zone at the pollen tube tip.

Loss of Function of ALA3 Alters the Distribution Pattern and the Amount of PS in Pollen Tubes

ALA3 was previously reported to flip phospholipids, including PE, PS, and PC, between two membrane leaflets (López-Marqués et al., 2010). However, the total content of phospholipids in *ala3* pollen was not obviously changed compared to that in wild-type pollen; thus, it was proposed that the phenotypes of *ala3* were caused by the disordered distribution of lipids (McDowell et al., 2013). Here, the C2 domain of bovine lactadherin (Lact-C2), which could mark PS on the cytoplasmic leaflet of the PM and the membrane of the organelles (Yeung et al., 2008), was used to mark PS in Arabidopsis pollen tubes. As shown in Figure 4, EGFP-Lact-C2-labeled PS was abundantly localized at the inverted-cone zone of the pollen tube and partially dotted the shank region of the pollen tube (Figure 4A). Next, by tracking its dynamic process, PS was shown to move fast, resembling the movement pattern of RabA4b-labeled vesicles (see Supplemental Movie 8). EGFP-Lact-C2 also colocalized with the membrane dye FM4-64 at the apical and shank regions of the pollen tube (Figures 4B to 4D). Furthermore, the colocalization between EGFP-Lact-C2 and various organelle markers was identified and quantified, and the results indicated that EGFP-Lact-C2 was mainly colocalized with markers of the TGN/EE (r_p was 0.18 and 0.42 in the tip and the shank, respectively), post-Golgi (r_p was 0.55 and 0.51 in the tip and the shank, respectively), and endosome (r_p was 0.56 and 0.54 in the tip and the shank, respectively; Figures 4E to 4K). Kymograph analysis showed the localization of spots in the two channels over time (Figures 4N to 4P; Supplemental Figure 7). The polarized localization of EGFP-Lact-C2 at the apical region could be seriously affected by endomembrane inhibitors (Supplemental Figure 8), suggesting that apical PS distribution also depended on endomembrane transport.

To identify the direct effect of ALA3 on PS distribution in pollen tubes, we crossed the *ala3* mutant with the above PS marker lines. In the *ala3* mutant, the polarized distribution of PS in the apical region of pollen tube dramatically decreased, chiefly accumulating in the subapical region, and PS fluorescent signals in both the apical and shank regions of the pollen tube were observably decreased (Figures 4L and 4M; see Supplemental Movies 9 and 10). In addition, the distributions of PS in wild type and *ala3* were almost consistent with those of vesicles labeled with FM4-64 or YFP-RabA4b (Figures 1A to 1D), and PS was also colocalized with RabA4b, RabD1, RabA1g, and FM4-64 in pollen tubes (Figures 4B to 4K). Thus, these results suggested that ALA3 plays a key role in the polarized distribution of PS at the pollen tube tip, and PS might regulate the localization and related vesicle trafficking of certain Rab GTPases.

Loss of Function of ALA3 Has a Negative Effect on TGN/EE Distribution in Pollen Tubes

In the *ala3* mutant, the fluorescence signals of vesicles labeled with FM4-64 and RabA4b/RabA4d were obviously decreased (Figures 1A to 1D and 3C to 3E), suggesting that ALA3 might also affect vesicle formation at the TGN/EE. To further clarify whether ALA3 affects TGN specially or regulates other subcellular compartments, we crossed the *ala3* mutant with different organelle markers and then quantified the fluorescence intensity of these markers. As shown in Figure 5 and Supplemental Figure 9,

Figure 1. (continued).

(E) Quantitative analysis of the percentage of apical-localized and subapical-localized YFP-RabA4b and the relative length of the growing pollen tube. The percentage of apical localization and subapical localization of YFP-RabA4b was calculated as the sum of the pixel intensities in the apical and subapical zones of the pollen tube compared with the sum of the pixel intensities in the entire pollen tube.

(F) and **(G)** Representative time-lapse trajectories of YFP-RabA4b at 5 s for Col-0 and *ala3* in the tip **(F)** and shank **(G)** zones of pollen tubes obtained by Imaris image analysis. Bars = 10 μm.

(H) Quantitative analysis of the relative vesicle velocity of YFP-RabA4b at the pollen tube tip **(F)** and shank **(G)** zones from Col-0 and *ala3*. The results represent the means ± SDS (n = 15). **P < 0.01 (*t* test compared to wild-type values).

(I) Growth of Col-0, *ala3*, *LAT52:ALA3-GFP;ala3*, and *ALA3:ALA3^{D413N};ala3* pollen tubes in vitro for 3 h. Bar = 30 μm.

(J) Quantitative analysis of the relative pollen tube width and length in Col-0, *ala3*, *LAT52:ALA3-GFP;ala3*, and *ALA3:ALA3^{D413N};ala3*. The results represent the means ± SDS (n = 100). **P < 0.01 (*t* test compared to wild-type values).

(K) Quantitative analysis of the relative length of Col-0 and *ala3* pollen tubes treated with BFA. The results represent the means ± SDS (n = 300). **P < 0.01 (*t* test compared to wild-type values).

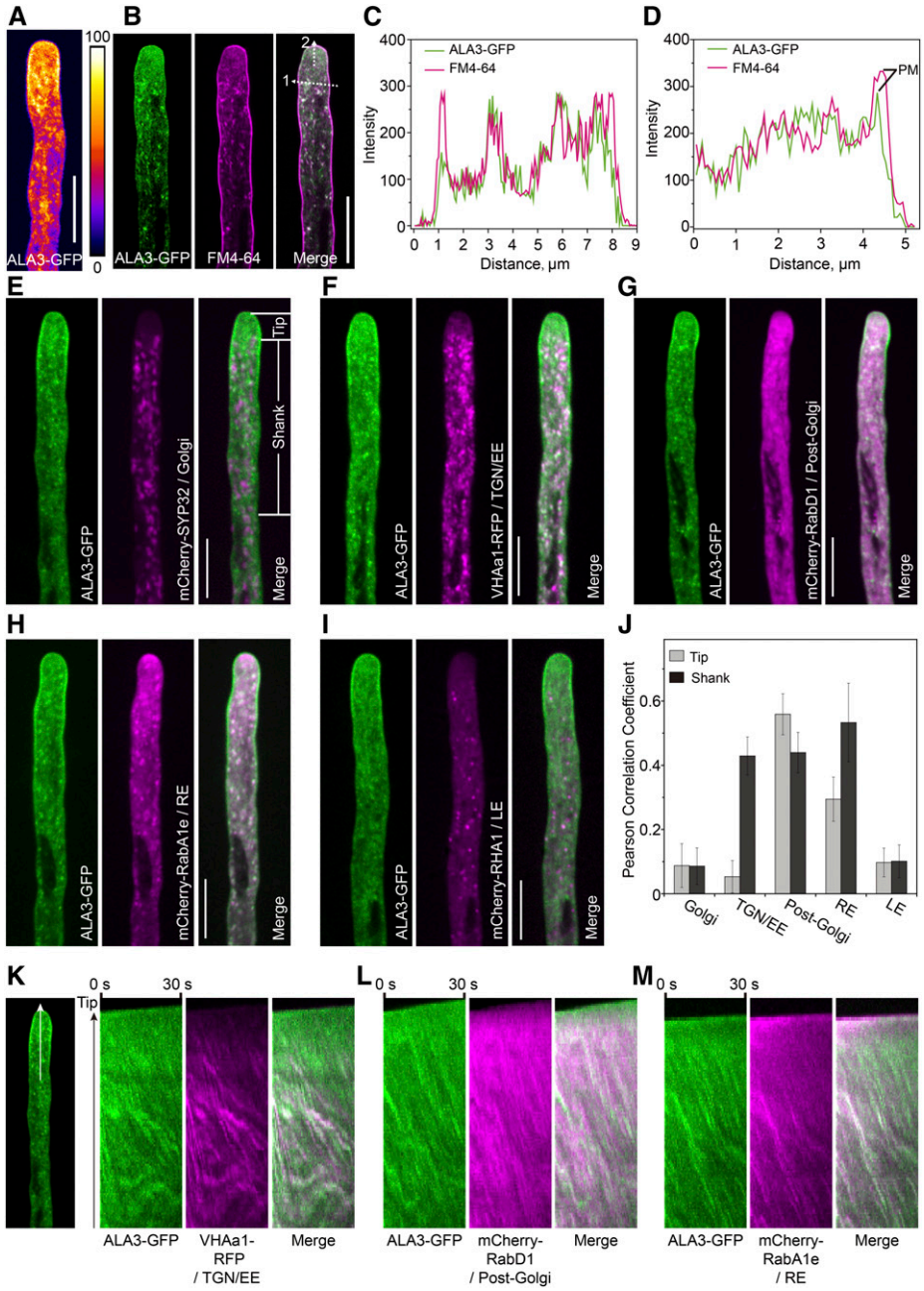

Figure 2. ALA3 Exhibits Polarized Distribution in Pollen Tubes and Is Localized to the Endomembrane and Plasma Membrane.

(A) Representative growing pollen tube from the *ala3* mutant expressing ALA3-GFP from the *LAT52:ALA3-GFP* transgene. Bar = 10 μm.
(B) Representative confocal images of a growing pollen tube expressing ALA3-GFP (green) with FM4-64 staining (magenta). Merged images are shown on the right. Bar = 10 μm.
(C) Line scan measurements (white dotted arrow 1) of the confocal image in **(B)** are plotted to show colocalization profiles.
(D) Line scan measurements (white dotted arrow 2) of the confocal image in **(B)** are plotted to show colocalization profiles. PM represents plasma membrane signals.
(E) to **(I)** Representative confocal images of growing pollen tubes coexpressing ALA3-GFP (green) with mCherry-SYP32 (Golgi) **(E)**, VHAa1-RFP (TGN/EE) **(F)**, mCherry-RabD1 (post-Golgi) **(G)**, mCherry-RabA1e (RE) **(H)**, or mCherry-RHA1 (LE) **(I)** (white). Merged images are shown on the right. Bars = 10 μm.
(J) Measurement of the Pearson correlation coefficient to reflect the colocalization level of ALA3-GFP with compartment markers. The tip and shank regions used for Pearson correlation coefficient measurement in here and the following pollen tubes are shown in **(E)**. The results represent the means ± SDs ($n = 15$).
(K) to **(M)** Kymograph representation of noncolocalized foci (green and magenta foci) and colocalized foci (white foci). The region used for Kymograph analysis in here and the following pollen tubes are shown on the left (white arrow).

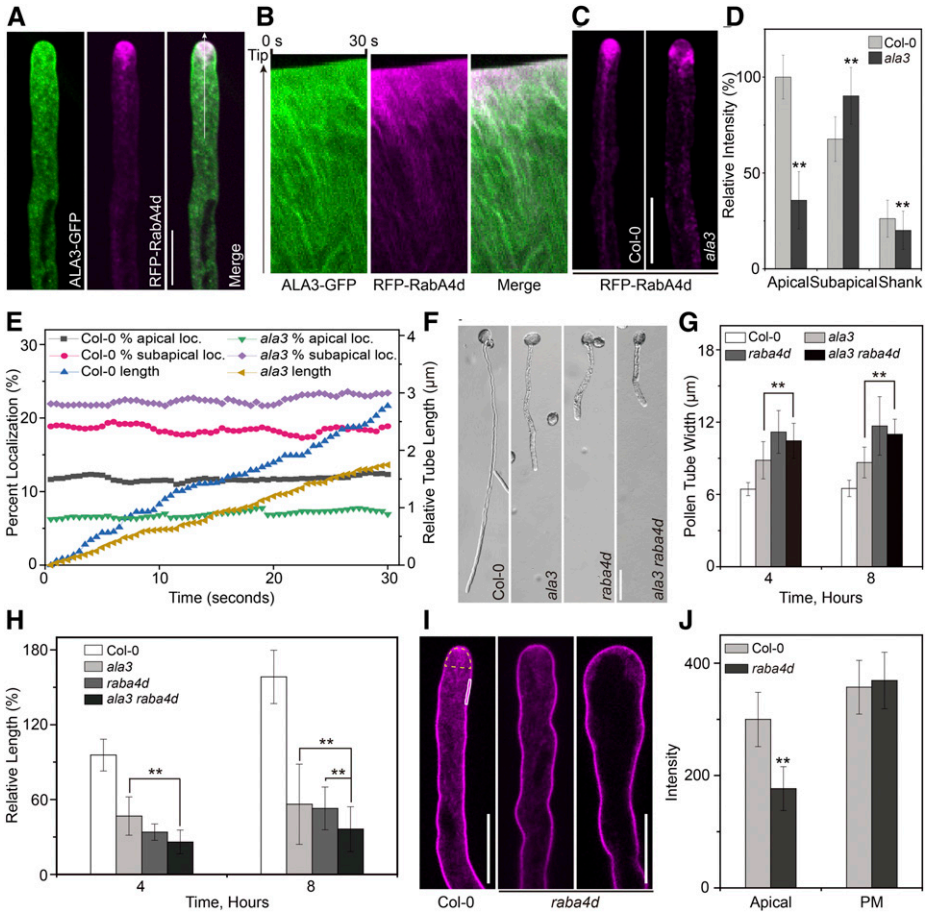

Figure 3. ALA3 and RabA4d Likely Collaborate to Regulate the Polarized Growth of Pollen Tubes.

(A) Representative confocal images of growing pollen tubes coexpressing ALA3-GFP (green) with RFP-RabA4d (magenta). Merged images are shown on the right. Bar = 10 μm.

(B) Kymograph representation of noncolocalized foci (green and magenta foci) and colocalized foci (white foci).

(C) Representative confocal images of growing pollen tubes from Col-0 and *ala3*-expressing RFP-RabA4d from the same transgenic line. Bar = 10 μm.

(D) Quantitative analysis of the relative fluorescence intensity of RFP-RabA4d in the apical, subapical, and shank zones of the pollen tube. The results represent the means ± SDS (n = 30). **P < 0.01 (t test compared to wild-type values).

(E) The percentage of apical-localized and subapical-localized RFP-RabA4d and the relative length of the growing pollen tube were measured. The percentage of apical localization and subapical localization of RFP-RabA4d was calculated as the sum of the pixel intensities in the apical and subapical zones of the pollen tube compared with the sum of the pixel intensities in the entire pollen tube.

(F) Growth of the Col-0, *ala3*, *raba4d*, and *ala3 raba4d* pollen tubes in vitro for 4 h. Bar = 30 μm.

(G) and **(H)** Quantification of pollen tube width **(G)** and relative pollen tube length **(H)** in Col-0, *ala3*, *raba4d*, and *ala3 raba4d*. The results represent the means ± SDS (n = 100). **P < 0.01 (t test).

(I) Representative confocal images of Col-0 and *raba4d* pollen tubes stained with FM4-64 for 20 min. Bars = 10 μm.

(J) Quantification of the fluorescence intensity of FM4-64 at the apical region and plasma membrane in Col-0 and *raba4d* pollen tubes. The regions used for fluorescence intensity measurement are marked in **(I)**. The apical region is marked in yellow, and the PM is marked in white. The results represent the means ± SDS (n = 30). **P < 0.01 (t test compared to wild-type values).

compared with the wild type, the distribution pattern and fluorescence intensity of the ER and Golgi markers HDEL-GFP and mCherry-SYP32 in *ala3* were not changed, suggesting that loss of function of ALA3 had no effect on these two organelles (Supplemental Figure 9). Next, VHAa1-RFP and mCherry-VTI12, two well-documented TGN/EE markers, were used. We found that both the density and fluorescence intensity of these TGN/EE markers were observably decreased within the shank region of the pollen tube of *ala3* (Figures 5A to 5E). In addition, the movement velocities of these markers were comparable in the wild type and *ala3* mutant (Supplemental Figure 10). Interestingly, we found that there was no signal at the apical region of pollen tube with VHAa1-RFP in wild type, but the TGN/EE labeled with mCherry-VTI12 still exhibited some fast-moving small particles at the pollen tube tip, which were similar to FM4-64-labeled vesicles (Figures 5A and 5C; see Supplemental Movies 11 and 12). Additionally, the mCherry-

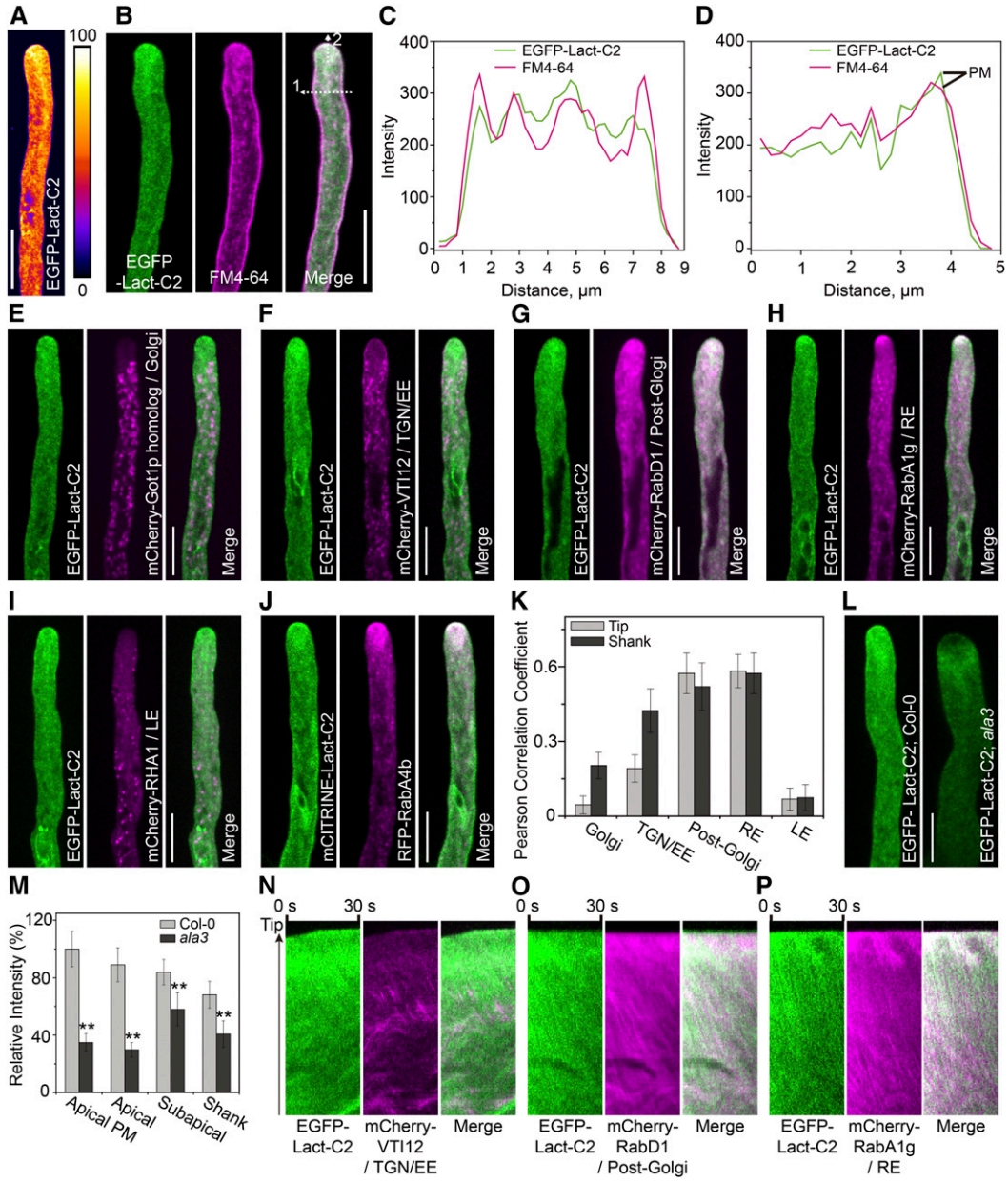

Figure 4. Loss of Function of ALA3 Alters the Distribution Pattern of PS.

(A) Representative growing pollen tube from Col-0 expressing EGFP-Lact-C2 from the *LAT52:EGFP-Lact-C2* transgene. Bar = 10 μm.

(B) Confocal images of a growing pollen tube expressing EGFP-Lact-C2 (green) stained with FM4-64 (magenta) for 20 min. Merged images are shown on the right. Bar = 10 μm.

(C) Line scan measurements (white dotted arrow 1) of the confocal image in **(B)** are plotted to show colocalization profiles.

(D) Line scan measurements (white dotted arrow 2) of the confocal image in **(B)** are plotted to show colocalization profiles. PM represents plasma membrane signals.

(E) to **(J)** Representative confocal images of growing pollen tubes coexpressing EGFP-Lact-C2 or mCITRINE-Lact-C2 (green) with the mCherry-Got1p homolog (Golgi) **(E)**, mCherry-VTI12 (TGN/EE) **(F)**, mCherry-RabD1 (post-Golgi) **(G)**, mCherry-RabA1g (RE) **(H)**, mCherry-RHA1 (LE) **(I)** or RFP-RabA4b (r_p = 0.42) **(J)** (magenta). Merged images are shown on the right. Bars = 10 μm.

(K) Measurement of the Pearson correlation coefficient to reflect the colocalization level of EGFP-Lact-C2 with compartment markers. The results represent the means ± SDS (n = 15).

(L) Representative confocal images of growing pollen tubes from Col-0 and *ala3*-expressing EGFP-Lact-C2 from the same transgenic line. Bar = 10 μm.

(M) Quantification of the relative fluorescence intensity of EGFP-Lact-C2 in Col-0 and *ala3* pollen tubes. The results represent the means ± SDS (n = 30). **P < 0.01 (t test compared to wild-type values).

(N) to **(P)** Kymograph representation of noncolocalized foci (green and magenta foci) and colocalized foci (white foci).

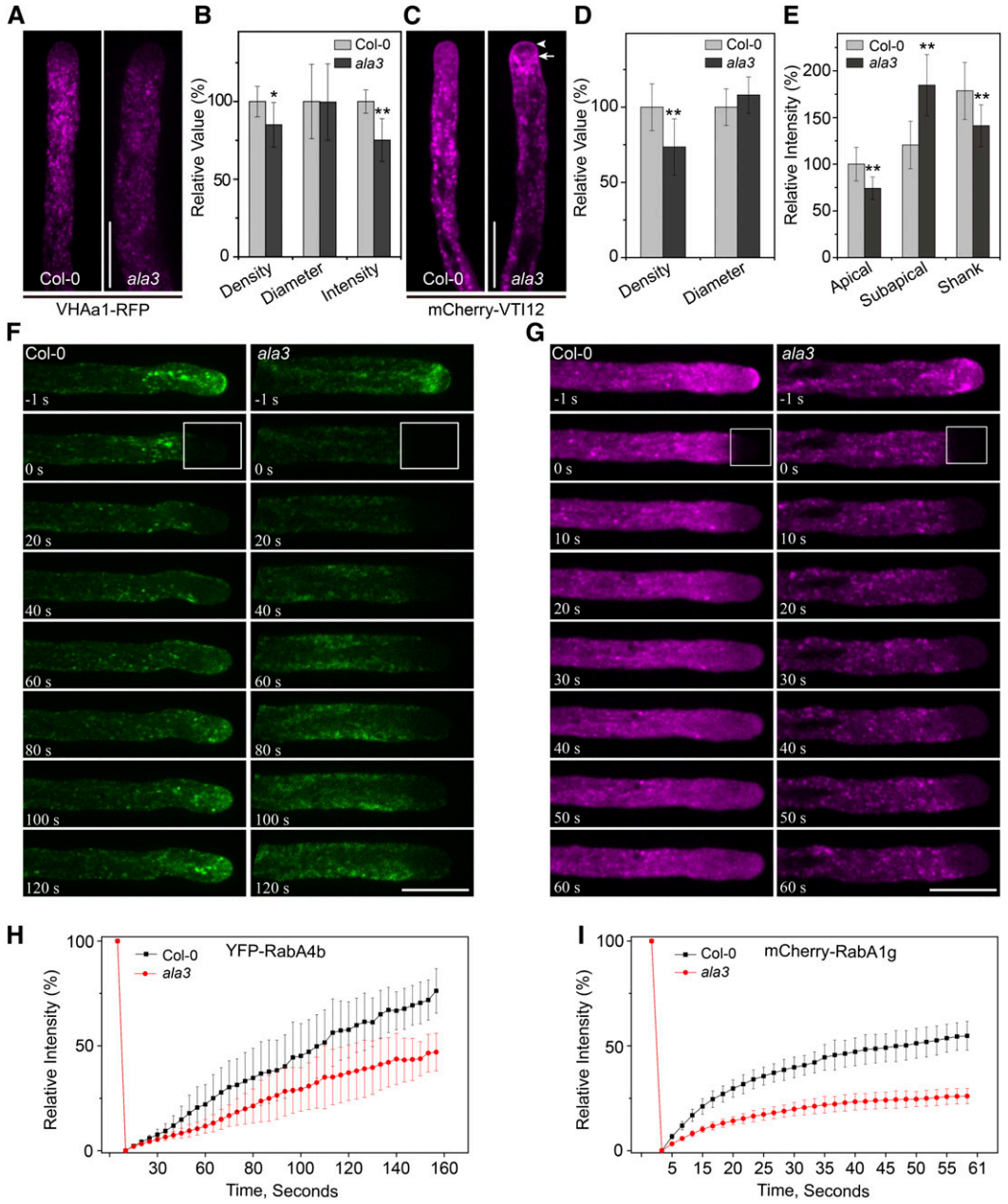

Figure 5. Loss of ALA3 Leads to Abnormal Distribution of the TGN/EE in Pollen Tubes.

(A) Representative confocal images of growing pollen tubes from Col-0 and *ala3*-expressing VHAa1-RFP from the same transgene. Bar = 10 μm.
(B) Quantification of the relative puncta density, diameter, and fluorescence intensity marked by VHAa1-RFP in Col-0 and *ala3* pollen tubes. The results represent the means ± SDS (n = 30). *P < 0.05; **P < 0.01 (t test compared to wild-type values).
(C) Representative confocal images of growing pollen tubes from Col-0 and *ala3*-expressing mCherry-VTI12 from the same transgenic line. The arrowhead and arrow indicate the apical and subapical zones, respectively. Bar = 10 μm.
(D) Quantification of the relative puncta density and diameter marked by mCherry-VTI12 in Col-0 and *ala3* pollen tubes. The results represent the means ± SDS (n = 30). **P < 0.01 (t test compared to wild-type values).
(E) Quantification of the relative fluorescence intensity of mCherry-VTI12 in Col-0 and *ala3* pollen tubes. The results represent the means ± SDS (n = 30). **P < 0.01 (t test compared to wild-type values).
(F) Fluorescence recovery after photobleaching (FRAP) analysis of YFP-RabA4b in growing pollen tubes. The time points after photobleaching are labeled in each image. The bleached area is marked by the box. Bar = 10 μm.
(G) FRAP analysis of mCherry-RabA1g in growing pollen tubes. The time points after photobleaching are labeled in each image. The bleached area is marked by the box. Bar = 10 μm.
(H) Measurement of the mean YFP fluorescence intensity of the bleached area in **(F)**. The results represent the means ± SDS (n = 7).
(I) Measurement of the mean mCherry fluorescence intensity of the bleached area in **(G)**. The results represent the means ± SDS (n = 7).

VIT12 signal at the apical region of the pollen tube dramatically decreased and moved to the subapical region in *ala3*, similar to the markers FM4-64, RabA4b/4d, and EGFP-Lact-C2 (Figures 5C and 5E; see Supplemental Movies 13 and 14). Thus, our data provide evidence that VTI12 could also mark other vesicles and endomembrane compartments in addition to the TGN/EE. Next, we performed fluorescence recovery after photobleaching (FRAP) analysis to examine the fluorescence recovery of YFP-RabA4b and mCherry-RabA1e. As shown in Figures 5F to 5I, the recovery rates of YFP-RabA4b and mCherry-RabA1e in *ala3* were much slower than those in the wild type, indicating that lack of ALA3 function had a significant influence on secretory vesicle recycling. Based on these results, it is possible that ALA3 was also involved in regulating the TGN/EE to reduce the number of secretory vesicles and had an effect on their polarized distribution in the apical region of pollen tube.

Loss of Function of ALA3 Ultimately Leads to Aberrant Composition of the Cell Wall of Pollen Tubes

RabA4d-mediated vesicle trafficking delivers indispensable cargoes, such as cell wall components, for the polar growth of pollen tubes (Szumlanski and Nielsen, 2009). Therefore, we determined the cell wall composition of the pollen tube of the *ala3* mutant. As shown in Figure 6, compared with wild type, the levels of arabinogalactan proteins, xyloglucan, and low-methyl-esterified homogalacturonan (HG), marked by LM2, LM15, and JIM5, were sharply reduced in the *ala3* pollen tube, while there was no significant change in the levels of rhamnogalacturonan I and high-methyl-esterified HG between the wild type and the mutants labeled with LM6 and JIM7, respectively (Figures 6A and 6B). Additionally, the activity of callose synthase was mainly present at the PM near the apical region and spread to the shank of the pollen tube, but the cell wall stained with aniline blue was not changed (Figures 6C and 6D). Another enzyme expressed in pollen grains and pollen tubes is the pectin methylesterase VANGUARD1 (VGD1), the function of which could affect the ratio of low HG to high HG to promote pollen tube growth. In our work, the VGD1-GFP signal in the *ala3* pollen tube also dramatically decreased (Figures 6E and 6F). Taken together, these results indicated that loss of function of ALA3 caused a defect in cell wall transport, which in turn induced alterations in the cell wall components of the pollen tube and finally had an adverse effect on the polar growth of the pollen tube.

ALA3 Principally Affects the Polarized Localization and Distribution of Secreted Rab GTPases at the Pollen Tube Tip

To further determine whether and how loss of function of ALA3 affects Rab GTPases in a wide variety of endomembrane transport pathways, we identified the localization pattern of Rab GTPases involved in different transport pathways in the wild type and *ala3*. RabA1e and RabA1g, which are known to specifically label recycling endosomes (REs), were located in the shank region and a smaller region close to the apical membrane of the pollen tube, and they also moved in an ordered and rapid manner between the shank and apical regions (Figures 7A to 7D; see Supplemental

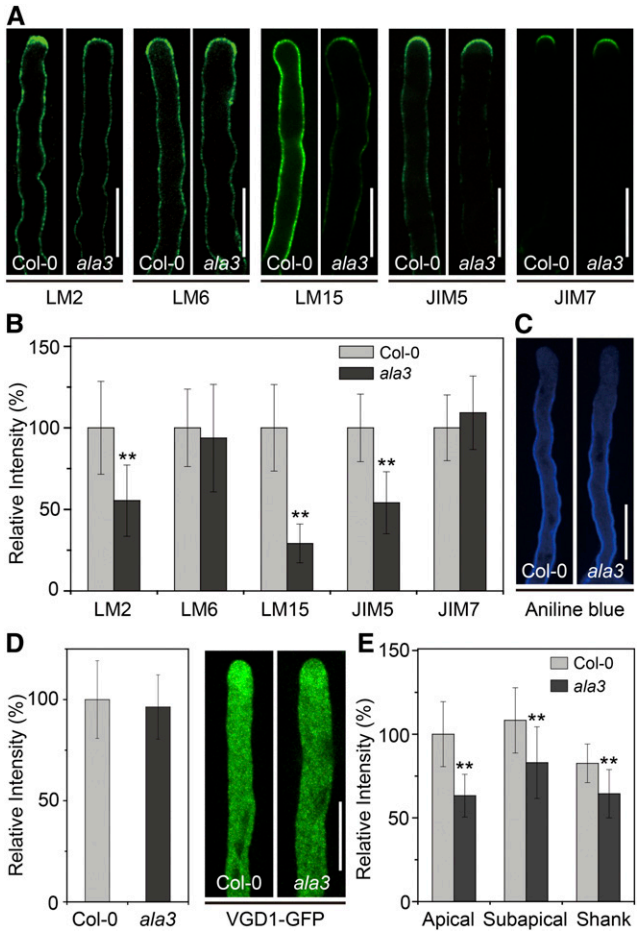

Figure 6. The Abundance of Cell Wall Components in the Pollen Tube Is Changed in *ala3*.

(A) Immunolabeling of cell wall components in Col-0 and *ala3* pollen tubes using LM2, LM6, LM15, JIM5, and JIM7. Bar = 10 μm.
(B) Quantitative analysis of the relative fluorescence intensity of the different cell wall epitopes indicated in Col-0 and *ala3* pollen tubes. The results represent the means ± SDS ($n = 30$). **$P < 0.01$ (*t* test compared to wild-type values).
(C) Aniline blue staining of the pollen tubes in Col-0 and *ala3*. Bar = 10 μm.
(D) Quantitative analysis of the relative fluorescence intensity of aniline blue in Col-0 and *ala3* pollen tubes. The results represent the means ± SDS ($n = 30$).
(E) Representative confocal images of growing pollen tubes from Col-0 and *ala3*-expressing VGD1-GFP from the same transgenic line. Bar = 10 μm.
(F) Quantitative analysis of the relative fluorescence intensity of VGD1-GFP in Col-0 and *ala3* pollen tubes. The results represent the means ± SDS ($n = 30$). **$P < 0.01$ (*t* test compared to wild-type values).

Movies 15 and 16). However, in *ala3*, the polarized localization of these two proteins dramatically decreased, and the fluorescence intensity prominently decreased; these proteins mainly accumulated in the two flanks of the subapical region with irregular activities (Figures 7A to 7D; see Supplemental Movies 17 and 18). The results indicate that ALA3 had a marked influence on both the polarized localization and distribution of RabA1e and RabA1g. Interestingly, although RabA5d also colocalized with REs, the

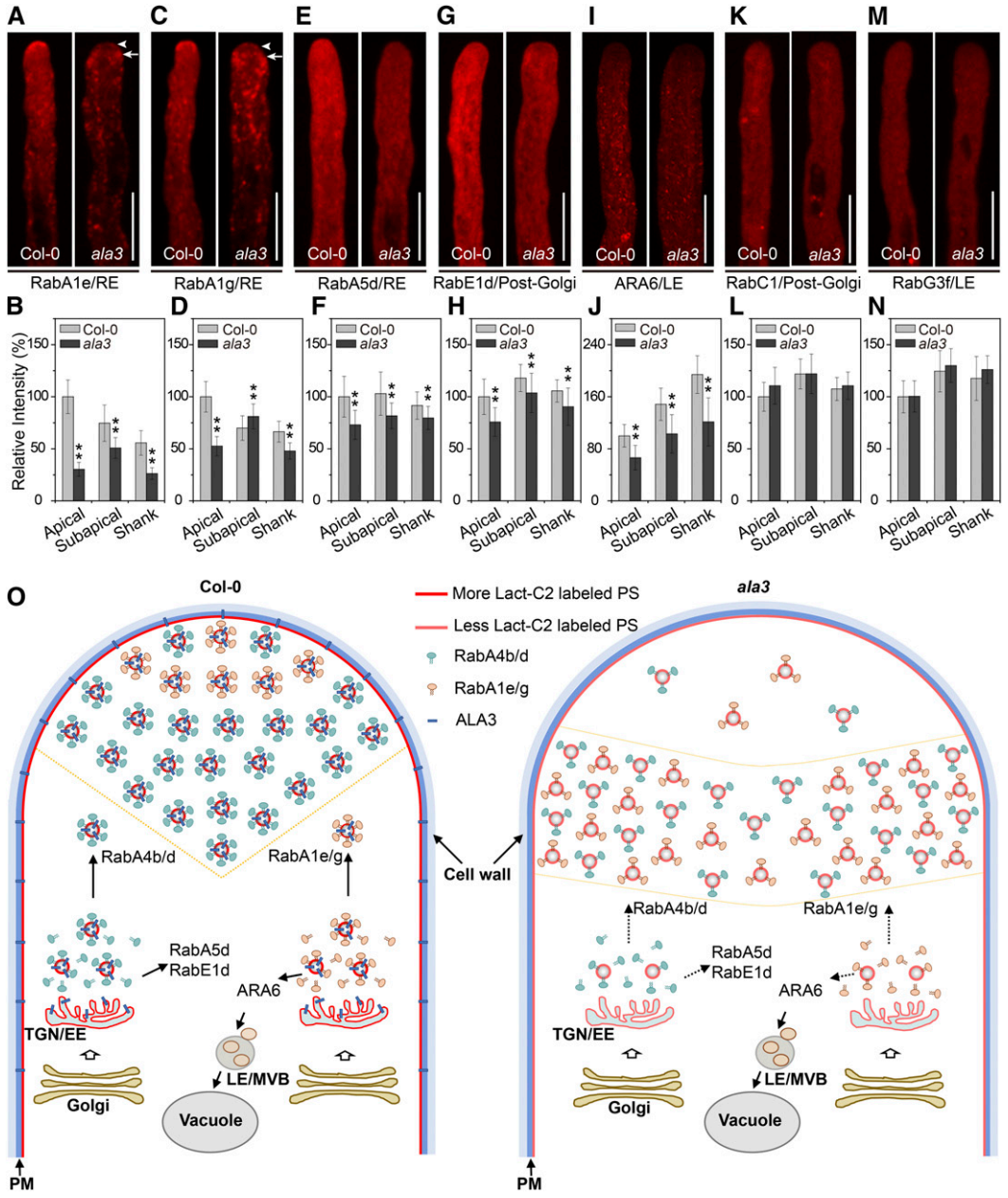

Figure 7. The Localization and Distribution of Secreted Rab GTPases in the Pollen Tube Are Changed in *ala3*.

(A), **(C)**, **(E)**, **(G)**, **(I)**, **(K)**, **(M)** Representative confocal images of growing pollen tubes from Col-0 and *ala3*-expressing mCherry-RabA1e (RE) **(A)**, mCherry-RabA1g (RE) **(C)**, mCherry-RabA5d (RE) **(E)**, mCherry-RabE1d (post-Golgi) **(G)**, RFP-ARA6 (LE) **(I)**, mCherry-RabC1 (post-Golgi) **(K)**, or mCherry-RabG3f (LE) **(M)** from the same transgene. The arrowhead and arrow indicate the apical and subapical zones, respectively. Bars = 10 μm.

(B), **(D)**, **(F)**, **(H)**, **(J)**, **(L)**, **(N)** Quantitative analysis of the relative fluorescence intensity of mCherry-RabA1e (RE) **(B)**, mCherry-RabA1g (RE) **(D)**, mCherry-RabA5d (RE) **(F)**, mCherry-RabE1d (post-Golgi) **(H)**, RFP-ARA6 (LE) **(J)**, mCherry-RabC1 (post-Golgi) **(L)**, and mCherry-RabG3f (LE) **(N)** in Col-0 and *ala3* pollen tubes. The results represent the means ± SDS ($n = 30$). **$P < 0.01$ (*t* test compared to wild-type values).

(O) A model was proposed for the role of ALA3 in the polarized distribution of PS and vesicle trafficking. In Col-0 pollen tubes, ALA3 is required for the polarized distribution of PS, which regulates the distribution and activity of certain Rab GTPases. In *ala3* pollen tubes, the total PS level at the cytosolic leaflet decreases significantly, and PS accumulates in the subapical zone, causing reduced vesicle formation and accumulation of vesicles in the subapical zone. The mislocalization of vesicles causes failed secretion, leading to pollen tube growth defects.

fluorescence intensity of mCherry-RabA5d decreased in both the apical and shank regions in the *ala3* mutant (Figures 7E and 7F), but its distribution pattern was not changed. In addition, RabE1d and RabC1, which are post-Golgi markers, were located in the whole pollen tube and moved rapidly in the apical region. We found that the fluorescence intensity of RabE1d was reduced in *ala3* (Figures 7G and 7H). However, the fluorescence intensity of RabC1, as well as the distribution pattern of these two markers, were unchanged in *ala3* compared with the wild type (Figures 7K and 7L). Likewise, ARA6 and RabG3f are two specific LE markers that were limited at the shank region of the pollen tube. The fluorescence intensity of ARA6 was obviously weakened, but its distribution pattern was not changed in *ala3* (Figures 7I and 7J). Unlike ARA6, both the fluorescence intensity and distribution pattern of RabG3f were unchanged (Figures 7M and 7N). In conclusion, we found that the functional deficiency of ALA3 affected multiple Rab GTPase-mediated vesicle transport pathways, but the regulatory mechanisms for Rab GTPases in various transport pathways were different.

DISCUSSION

PS Is Abundantly Localized in the Inverted-Cone Zone of the Arabidopsis Pollen Tube

The asymmetric distribution of PS between the two biomembrane leaflets has a profound influence on the surface charge, curvature, and lipid packing of the PM and specific endomembrane, as well as the electrostatic gradient among different intracellular compartments (Yeung et al., 2008; Muthusamy et al., 2009; Xu et al., 2013; Platre et al., 2018). Thus, PS plays a crucial role in endomembrane trafficking. Here, we found that EGFP-Lact-C2-labeled PS was mainly located in the inverted-cone zone of the pollen tube in Arabidopsis, suggesting a potential correlation between the polarized distribution of PS and an accumulation of large amounts of post-Golgi-derived vesicles in the apical region of pollen tube. We also observed the localization of mCITRINE-Lact-C2-labeled PS in the pollen tube of Arabidopsis (Platre et al., 2019) and found that its localization pattern was similar to that of the EGFP-Lact-C2-labeled PS (Supplemental Figure 11). In addition, this polarized PS distribution in Arabidopsis pollen tubes was quite similar to that in root hairs as well as in tobacco pollen tubes (Platre et al., 2018). We therefore determined the subcellular localization of PS and found that PS was primarily enriched in the TGN/EE, vesicles, endosomes, and the PM in pollen tubes (Figures 4B to 4K), which was consistent with the localization in root cells (Platre et al., 2018), indicating that the subcellular localization of PS in different cell types in planta are similar. Based on previous studies on anionic lipids in pollen tubes, it was known that LE/multivesicular body-localized PtdIns(3)P was involved in vesicle degradation (Vermeer et al., 2006; Jean and Kiger, 2012); PtdIns(4)P mainly accumulated at the PM of subapical and shank regions of pollen tubes and contributed to the endocytic process (Zhao et al., 2010); PtdIns(4,5)P_2 was also localized at the PM in both the apical and subapical regions and was reported to control the growing site and direction of pollen tube growth (Kost et al., 1999; Hempel et al., 2017); PA was also a PM-localized lipid in tobacco pollen tubes (Potocký et al., 2014). Furthermore, we noticed that PS was not only distributed chiefly in the inverted-cone zone of vesicle enrichment at the apical region of pollen tube but also colocalized with the vesicular markers RabA4b, RabA1g, and RabE1 or with the endocytic dye FM4-64 (Figures 4B to 4K), confirming that anionic lipids participate in the regulation of the polarized distribution and trafficking of vesicles at the apical region of pollen tube in various ways. In addition, it was reported that PI4P and PA were also located at the PM, while PS was accumulated at both the PM and endomembrane in dividing root cells (Platre et al., 2018). Taken together, these results show that PS probably plays an important role in endomembrane trafficking in different cell types in plants.

ALA3 Is a Key Regulator of PS Distribution and the Polarized Growth of Arabidopsis Pollen Tubes

Each member of the Arabidopsis ALA protein has its own tissue expression and subcellular localization patterns as well as specific lipid-flipping activity (Gomès et al., 2000; Poulsen et al., 2008; López-Marqués et al., 2010). However, which ALAs are involved in the polarized distribution and localization of PS in pollen tubes remains unknown to date. We revealed that *ALA3* was abundantly expressed in pollen grains (Supplemental Figure 3), and its distribution, movement trajectory, and subcellular localization were extremely similar to those of PS in the apical region of pollen tubes (Figures 2 and 4A to 4K). Additionally, a lack of ALA3 activity resulted in a significant decrease of PS in the apical region but aggregation in the subapical region and an apparent decrease in PS in the shank of the pollen tube (Figures 4L and 4M). Lact-C2 marks PS only on the cytoplasmic leaflet of the PM and the membranes of organelles (Yeung et al., 2008). In addition, ALA3 had been reported to have PS-flipping activity (López-Marqués et al., 2010), and the total content of PS in *ala3* pollen was not obviously changed (McDowell et al., 2013). Therefore, the main reason for the decrease of PS signal in the *ala3* mutant may be the lack of the PS-flipping activity of ALA3, leading to the failure of PS to effectively flip to the cytoplasmic side of the PM and organelles. Thus, we propose that ALA3 is a key member of the ALA family involved in establishing and maintaining the polarized distribution of PS in pollen tubes. Indeed, ALA3 might translocate PS from the extracellular/luminal leaflet of the membrane into the cytosolic leaflet when transported in a polarized pattern, causing polarized distribution of PS at the apical region of pollen tube with a highly dynamic pattern.

Previous studies have shown that ALA3 participates in many crucial physiological activities via multiple mechanisms, including root and pollen tube growth (Poulsen et al., 2008; McDowell et al., 2013; Zhang et al., 2020), trichome development (Zhang and Oppenheimer, 2009), and resistance to pathogens (Underwood et al., 2017). For example, in Arabidopsis root and tobacco leaf cells, ALA3 was reported to be localized mainly in the Golgi apparatus and only partially in the TGN/EE, and loss of function of ALA3 led to a defect in the production of secretory vesicles in root peripheral columella cells, which thereby inhibited root growth (Poulsen et al., 2008). The latest research has reported that ALA3, which is located mainly in the Golgi, TGN/EE, and PM, functions together with the ARF GTPase exchange factors (GNOM and

BIG3) in regulating PIN polarity, trafficking, and auxin-mediated development (Zhang et al., 2020). In addition, it was recently shown that loss of ALA3 function had a negative impact on the cycling of the defense protein PENETRATION3 between the PM and TGN/EE and subsequently affected plant immune responses against powdery mildews (Underwood et al., 2017). In addition, the reason for the slow growth rate of the *ala3* mutant pollen tube was proposed to be a change in the trajectory of cytoplasmic streaming (McDowell et al., 2013). Here, we found that loss of ALA3 resulted in increased pollen tube width and an absence of apical vesicle distribution, suggesting that ALA3 also played another important role in the polarity of pollen tube growth.

In contrast to the subcellular localization within root cells, ALA3 in pollen tubes is mainly located at the TGN/EE, vesicles, RE, and the PM but is scarcely colocalized with Golgi markers (Figure 2). This result was highly consistent with the fact that no ER and Golgi were present in the apical region of pollen tube (Cheung and Wu, 2008; Chebli et al., 2013; Supplemental Figure 9). Importantly, in the *ala3* pollen tube, the fluorescence intensity of the TGN/EE was observed to be significantly reduced; in addition, the amounts of secretory vesicles also decreased, and the vesicle secretion rate correspondingly decreased (Figure 5). Moreover, the transport direction of apical vesicles in the *ala3* pollen tube was severely affected; PS and other endomembrane-derived vesicles could not arrive at the apical region and moved in a disordered manner within the subapical region of the pollen tube. In addition, the polarized distribution of ALA3 and PS in the apical region of pollen tube was highly sensitive to several trafficking inhibitors, including BFA, Wort, and LatB (Supplemental Figures 5 and 8). Furthermore, we also measured the uptake of FM4-64 in Col-0 and *ala3* pollen tubes over time, and we found that the levels of internalized FM4-64 in Col-0 and *ala3* were similar at 5 min, indicating that the endocytosis is not affected in the *ala3* mutant (Supplemental Figure 12).

In summary, ALA3 was confirmed to be closely associated with post-Golgi-mediated vesicular secretion and polarized transport at the apical region of pollen tube, and the altered transport direction of apical vesicles was suggested to be the primary reason for the defects in the polar growth of the *ala3* pollen tube. Interestingly, Zhang and Oppenheimer (2009) reported that the pollen tubes in *ala3* grew slowly, but the root hair length was relatively high, indicating that ALA3 had pleiotropic effects in different types of polar cells. Based on these results, we proposed that the subcellular localization and functional mechanism of ALA3 varied among different cell types in plants.

PS Might Be a Potential Phospholipid Signaling Molecule Regulating Polarized Transport at the Apical Region of Pollen Tubes

Rab GTPases constitute a key functional protein family that contributes to endomembrane trafficking in eukaryotes and can recognize and bind to specific organelles and the PM to participate in multifarious transport pathways via varying molecular mechanisms (Nielsen et al., 2008; Woollard and Moore, 2008; Kjos et al., 2018). Therefore, the specificity of Rab protein localization is the basis for its biological function. However, the molecular mechanisms regulating Rab GTPase localization have proved tricky issues to address. Numerous studies have shown that the localization and distribution of Rabs are directly regulated by multiple factors, including guanine-nucleotide-exchange factors, GTPase-activating proteins, effector proteins, interacting proteins, and phosphoinositides (Zerial and McBride, 2001; Grosshans et al., 2006; Thomas et al., 2019). Here, the vesicles labeled with FM4-64, RabA4b/4d, RabA1e, and RabA1g could not reach the apical region of pollen tubes of the *ala3* mutant; and the vesicles clustered in the subapical region of the pollen tube in a disordered manner (Figures 1A to 1D, 3A to 3E, and to D7A to 7D). These results showed that ALA3 was involved in establishing the polarized localization of these vesicles in the apical region of pollen tubes. Moreover, we found that PS colocalized with RabA4b, RabD1, and RabA1g in pollen tubes (Figures 4E to 4K). The evidence from genetic analysis showed that ALA3 and RabA4d were collectively responsible for regulation of the polar growth of pollen tubes (Figure 3). Based on these results, we propose that PS likely acts as a signaling molecule to participate in the polarized distribution and transport of Rab GTPase-mediated vesicles at the apical region of pollen tube.

Recently, Platre et al. (2019) reported that PS directly binds to another important small GTPase, termed Rho of Plants 6 (ROP6), in vitro and in vivo; PS could recruit ROP6 into nanodomains in specific membrane regions and had a notable effect on polar auxin transport and gravitropism in roots. We also conducted the same lipid overlay experiments in vitro and found that ROP6, RabA4b, RabA4d, RabD1, and RabA1g could bind to PS and certain other anionic lipids in vitro (Supplemental Figures 13D to 13H). In addition, to verify whether different forms of Rab GTPases have different phospholipid binding activity, we also improved the experiment by expressing the constitutively active and dominant-negative forms of RabA4d (RabA4d^{Q74L} and RabA4d^{T29N}), RabA4b (RabA4b^{Q76L} and RabA4b^{S31N}), and RabD1 (RabD1^{Q67L} and RabD1^{S22N}). The results of lipid overlay experiments showed that either constitutively active or dominant-negative forms of these Rab GTPases could bind to PS and the other anionic lipids (Supplemental Figures 13I to 13N). Then, a liposome cosedimentation assay was performed to quantify the phospholipid binding activity of different forms of RabA4d. We found that RabA4d^{Q74L} and RabA4d exhibited comparable binding activities to PS; however, RabA4d^{T29N} exhibited slightly increased binding activity to PS compared to RabA4d^{Q74L} and RabA4d (Supplemental Figures 14A to 14E). Moreover, the binding activity of RabA4d to PI4P was higher than that to PS (Supplemental Figures 14F and 14G). Thus, we hypothesized that the polarized distribution of PS might have a direct influence on the polarized localization of these Rab GTPases as well as of their targeted vesicles at the pollen tube tip. These findings indicate the existence of a new mechanism by which PS regulates vesicle trafficking. However, Rop1 was found to be localized at the apical PM of the pollen tube, which was chiefly involved in regulating the growth direction of the pollen tube (Fu et al., 2001; Luo et al., 2017), indicating that PS probably had specific regulatory mechanisms for distinct small GTPases (Figure 7O).

Furthermore, lipid binding assays demonstrated that Rab GTPases could also bind to other anionic lipids, such as PA and PIPs, in addition to PS (Supplemental Figure 13). Liposome cosedimentation assays also demonstrated that RabA4d cannot

bind to PE and PC in vitro, which is consistent with the results of lipid overlay experiments (Supplemental Figure 14). Because PIPs have been confirmed to affect the localization of Rab GTPases by regulating many effector proteins (Jean and Kiger, 2012; Noack and Jaillais, 2017), it was suggested that the localization and function of Rab GTPases in pollen tubes were also likely regulated by these anionic lipids. Based on these results, we proposed that Rab GTPases might bind to these anionic lipids for preliminary localization, and Rab guanine-nucleotide-exchange factors or other effector proteins likely affect the subsequent precise localization of Rab GTPases. In addition, PI4Ks have been proven to be important effectors of RabA4 family, which plays an important role in the polar growth of pollen tubes and root hairs (Thole et al., 2008; Szumlanski and Nielsen, 2009). The polar distribution of RabA4d/RabA4b in the tip of pollen tube of *ala3* mutant decreased significantly, so the distribution of PI4Ks in *ala3* mutant may also be affected, which indirectly/directly leads to changes in the distribution and content of membrane phospholipids, such as PtdIns(4)P and PtdIns(4,5)P_2. Deciphering the underlying mechanism of these intracellular activities should be an important direction for future research.

METHODS

Plant Materials

Arabidopsis (*Arabidopsis thaliana*) ecotype Columbia-0 (Col-0) was used as the wild type. Transgenic plants used in this study were in the Col-0 background. The *ala3* (SALK_082157), *raba4d* (CS360297), *ala1* (SALK_056947), *ala6* (SALK_150173), *ala7* (SALK_125598), *ala9* (SALK_128495), and *ala12* (SALK_111498) T-DNA insertion mutant seeds were obtained from the Arabidopsis Biological Resource Center. The T-DNA insertion in *ala3* was identified by PCR using the primers ALA3LP, ALA3RP, and LBb1.3. The T-DNA insertion in *raba4d* was identified by PCR using the primers RabA4d-F, RabA4d-R, and LB1. Primers are described in the Supplemental Table. The single mutants *ala3* and *raba4d* were crossed to obtain the double mutant *ala3 raba4d*. Selection of transformed lines with an *ala3* background was conducted as previously described by Zhu et al. (2017). The previously reported transgenic lines used in this study included *UBQ10*, mCherry-*RabC1* (Geldner et al., 2009); *UBQ10*, mCherry-*RabG3f* (Geldner et al., 2009); *UBQ10*, mCherry-*Rha1* (Geldner et al., 2009); *UBQ10*, mCherry-*VTI12* (Geldner et al., 2009); *UBQ10*, mCherry-*Got1p homolog* (Geldner et al., 2009); *UBQ10*, mCherry-*SYP32* (Geldner et al., 2009); *UBQ10*, mCherry-*RabA5d* (Geldner et al., 2009); *UBQ10*, mCherry-*RabD1* (Geldner et al., 2009); *UBQ10*, mCherry-*RabE1d* (Geldner et al., 2009); *UBQ10*, mCherry-*RabA1e* (Geldner et al., 2009); *UBQ10*, mCherry-*RabA1g* (Geldner et al., 2009); *UBQ10*, mCherry-*MEMB12* (Geldner et al., 2009); *LAT52*, *YFP-RabA4b* (Zhang et al., 2010); *UBQ10*, *mCITRINE-Lact-C2* (Platre et al., 2019); and *VHAa1:VHAa1-RFP* (Dettmer et al., 2006).

Growth Conditions

Seeds were vernalized for 3 d at 4°C after surface sterilization and then grown on Murashige and Skoog medium with 1% (w/v) agar. Seven-day-old seedlings grown on Murashige and Skoog medium were transferred to mixed soil in a greenhouse with a 16 h light/8 h dark photoperiod with white fluorescent light (bulb type, TCL, TCLMY-28, 28 W, with five tubes; 100 μmol m^{-2} s^{-1}) and 65% relative humidity at 22 $\pm$ 2°C.

GUS Staining

The *ALA3* putative promoter, including the 1895-bp fragment upstream of the start codon, was amplified from Col-0 genomic DNA by PCR. Primers are described in the Supplemental Table. The fragment was cloned into the *pDONR/zeo* entry vector, and then the fragment was transferred into *pBIB-BASTA-GWR-GUS* binary vectors using LR Clonase II (Invitrogen). The T2-generation homozygous transgenic seedlings of *ALA3:GUS* were subjected to GUS (β-glucuronidase) staining. GUS staining procedures were performed as previously described by Jia et al. (2013). Images were obtained using a ZEN2 microscope equipped with ZEN 2.3 software (Carl Zeiss).

RT-PCR

Mature pollen grains of Col-0, *ala3*, the *LAT52:ALA3-GFP;ala3* complemented line, and the *ALA3:ALA3^{D413N};ala3* complemented line were collected. For mature pollen grain collection, at least 2 mL of fresh opened flowers were collected in a 5-mL tube, and then, 2 mL of 2% (w/v) Suc solution was added and vortexed for 1 min. The samples were centrifuged at 6000*g* for 2 min. The flowers and solutions were removed, and then the tubes with pellets (pollen grains) were saved in liquid nitrogen. Total RNA of the pollens was extracted using the MiniBEST plant RNA extraction kit (TaKaRa). Total cDNA was obtained through reverse transcription using M-MLV (RNase H^-) reverse transcriptase (TaKaRa). To confirm the *ALA3* expression levels in Col-0, *ala3*, and the complemented lines, the *ALA3* fragment was amplified from the total cDNA template by PCR. *EF4A* cDNA was amplified as the internal control. Primers are described in the Supplemental Table.

Pollen Tube Growth Analysis

For in vitro pollen tube growth, pollen from freshly opened flowers was smeared onto solid pollen germination medium as described previously by Zhu et al. (2017). Pollen tube length and width were measured using ImageJ software (http://rsbweb.nih.gov/ij/). To confirm the pollen tube growth rate in vivo, fresh pollen grains were pollinated onto the Col-0 pistils, the pistils were fixed for 2 h with ethanol/acetic acid (3:1) after pollination for 5 or 9 h, and a graded ethanol series of 80% (v/v), 50% (v/v), 30% (v/v), and double-distilled water were used to rehydrate the pistils. For softening, the pistils were incubated with 8 M NaOH overnight at 22°C and then washed at least three times with double-distilled water. Samples were then stained with aniline blue staining solution (0.1% [w/v] aniline blue in 100 mM phosphate buffer, pH 8.0) for at least 3 h in the dark. Images were obtained using a spinning-disk confocal microscope (Andor). Pollen tube length was measured using ImageJ software.

Gene Cloning and Plasmid Construction

The coding sequences of *ALA3*, *ARA6*, *RabA4d*, and *RabA4b* and the full-length genomic sequence of *VGD1* were amplified from the Col-0 cDNA library or genomic DNA by PCR. The coding sequence of *ALA3* with a point mutation (*ALA3^{D413N}*) was amplified by fusion PCR. The C2 domain of the lactadherin (*Lact-C2*) fragment with a stop codon was artificially synthesized. The coding sequence of *Lact-C2* was fused at the C terminus of *EGFP* to generate *EGFP-Lact-C2*. The coding sequences of *ALA3* and *EGFP-Lact-C2* were cloned into the *pDONR/zeo* entry vector and then transferred into the *pBIB-BASTA-LAT52-GWR-GFP* vector. The coding sequence of *ALA3^{D413N}* with a stop codon was cloned into the *pDONR/zeo* entry vector and then transferred into the *pBIB-HYG-pALA3-GWR* vector. The coding sequence of *ARA6* was cloned into the *pDONR/zeo* entry vector and then transferred into the *pBIB-BASTA-LAT52-RFP-GWR* vector. The coding sequences of *RabA4b* and *RabA4d* were cloned into the *pDONR/zeo* entry vector and then transferred into the *pBIB-BASTA-LAT52-RFP-GWR* vector. The full-length genomic sequence of *VGD1* was cloned into the *pDONR/zeo* entry vector and then transferred into the *pBIB-HYG-GWR-GFP* vector. To construct *LAT52:HDEL-GFP*, the ER retention signal *HDEL*

was subcloned from the *LAT52:AtbCH:EYFP:HDEL:NOS* vector by digesting the *Hind*III and *Xba*I sites and fused to the *pCAMBIA1300-LAT52:GFP* vector. These constructs were then transformed by *Agrobacterium tumefaciens* strain GV3101-mediated transformation into *ala3* homozygous mutants or the wild type. Transgenic plants were selected on hygromycin or Basta. All PCR amplifications were performed using PrimeSTAR GXL DNA polymerase (TaKaRa). Sequencing analyses were performed to confirm the amplified fragments. The primers used for the above cloning are described in the Supplemental Table.

Confocal Microscopy and Image Analysis

Confocal images of pollen tubes on solid pollen germination medium were acquired using a spinning-disk confocal microscope equipped with an iXON ultra EMCCD camera (Andor) as previously reported by Qu et al. (2013). Samples were observed using a 63× NA oil immersion lens. Image acquisition was performed using Andor IQ3 software. Time-lapse images were captured every 0.5 s to 1 s for 20 s to 2 min. GFP was excited with a 488-nm laser and observed using a 514-nm emission filter. YFP, mCITRINE was excited with a 514-nm laser and observed using a 542-nm emission filter. RFP, mCherry and FM4-64 were excited with a 561-nm laser and observed using a 607-nm emission filter. Images were quantified with ImageJ software. For colocalization evaluations, ImageJ with the Colocalization Finder plugin was used to calculate the Pearson correlation coefficients.

Quantification of the Velocity and Trajectory of Vesicle Movement

Imaris software was used to analyze the average trajectory speed. The parameters of the Imaris program were defined as follows: vesicles with an average diameter of 0.5 μm were labeled, the maximum distance between frames was 2 μm, the maximum gap size was 3, and the trajectory duration was 3 s.

Pharmacological Treatments

To determine the sensitivity of pollen tube growth to BFA, LatB, or Wort, a final concentration of 0.4 or 0.5 μM BFA, 1 or 2 nM LatB, or 0.6 or 1 μM Wort was added to the pollen germination medium. The same dilution ratio of DMSO was added as a control. After growth for 3 h, paraformaldehyde at a final concentration of 4% (w/v) in pollen germination medium was added to fix the samples before measuring pollen tube length. To determine the effects of inhibitors on ALA3-GFP and EGFP-Lact-C2 distribution in pollen tubes, a final concentration of 0.4 μM BFA, 1 nM LatB, or 1 μM Wort corresponding to 5 μM FM4-64 was added.

Aniline Blue Staining of Pollen Tubes

Pollen germinated for 3 h in vitro was fixed by using a fixative (4% [w/v] paraformaldehyde in liquid pollen germination medium, pH 7.0) and then washed three times with 100 mM phosphate buffer. Samples were stained directly with aniline blue staining solution for 5 min before microscopy.

FM4-64 Staining

After germination for 3 h on pollen germination medium, a final concentration of 5 μM FM4-64 was added. Pollen tubes were subjected to time-lapse imaging at the appropriate time point.

Immunolabeling

Immunolabeling of pollen tube cell wall epitopes was performed with LM2, LM6, LM15, JIM5, and JIM7 as described previously by Fabrice et al. (2018). Pollen tubes grown for 3 h on solid pollen germination medium were fixed by using a fixative (4% [w/v] paraformaldehyde, 50 mM PIPES buffer [pH 7.0], 2 mM $CaCl_2$, 3 mM $MgSO_4$, 18% [w/v] Suc) for 0.5 h at room temperature (RT). Samples were washed three times with PBS (137 mM NaCl, 2.7 mM KCl, 8 mM Na_2HPO_4, and 2 mM KH_2PO_4) for 5 min each and then blocked with 3% (w/v) BSA in PBS for 1 h at RT or overnight at 4°C. Samples were incubated for 1 h at RT with 1% (v/v) rat primary antibody (LM2, LM6, LM15, JIM5, JIM7) in PBS with 3% (w/v) BSA. Samples were washed three times with the same buffer and incubated with 0.5% (v/v) anti-rat IgG (whole molecule)-fluorescein isothiocyanate antibody (Sigma Aldrich; F1763) in PBS with 3% (w/v) BSA in the dark for 1 h at RT. Samples were washed five times for 5 min each with PBS, and then slides were mounted with mounting solution (50% [v/v] glycerol, 0.1% [w/v] p-phenylenediamine, and PBS) and observed with a spinning-disk confocal fluorescence microscope (Andor).

FRAP Analysis

FRAP experiments were performed using a spinning-disk confocal fluorescence microscope (Andor) equipped with a 63× NA oil immersion lens. The region of interest was bleached with a 488-nm argon laser at 100% transmission for 5 s. Fluorescence recovery was recorded at 5-s intervals for up to 5 min. The recovery percentage of each time point was calculated using the following equation: $(I_t - I_s)/(I_a - I_s) \times 100$, where I_t is the fluorescence intensity at each time point, I_s is the initial fluorescence intensity after bleaching, and I_a is fluorescence intensity before bleaching (Luu et al., 2012).

Immunoblot Analysis

Ten microliters (100 ng) of purified protein was used to analyze protein purity by immunoblotting using 1:10,000 anti- glutathione S-transferase (GST) primary antibody (Abmart, M20007) and incubated at RT for 1 h. Then, 1:10,000 secondary anti-mouse IgG (whole-molecule)-peroxidase antibody (Sigma Aldrich, A9044) was applied at RT for 1 h. Images were obtained using chemiluminescence detection.

Protein Expression, Purification, and Lipid-Protein Overlay Assay

The cDNAs of *RabA4d*, *RabA4b*, *RabD1*, *ROP6*, and *RabA1g* were amplified from the Col-0, with the primers listed in the Supplemental Table. The primers used for site mutation of the constitutively active and dominant-negative forms of the Rab GTPases are also listed in the Supplemental Table. The PCR products were cloned into the *pMD19-T* vector and then cloned into the *pGEX 4T-1* destination vector. The expression plasmids were transformed into *Escherichia coli* Rosetta cells for protein expression. Purification of GST-tagged recombinant proteins was performed as previously described by Xiang et al. (2007). For lipid-protein overlay assays, PIP strips containing fifteen purified lipids (P-6001, Echelon Bioscience) were blocked in 3% (w/v) BSA in TBS-T (150 mM NaCl, 50 mM Tris, and 0.05% [v/v] Tween 20; pH 8.0) at RT for 3 h. The strips were then incubated with 2 μg/mL purified proteins in 10 mL of TBS-T with 3% (w/v) BSA at RT for 2 h. After incubation, the strips were washed three times for 10 min each with TBS-T, then incubated with 1:10,000 anti-GST primary antibody (Abmart, M20007) in 10 mL TBS-T at RT for 1 h, then washed three times for 10 min each with TBS-T and incubated with 1:10,000 secondary anti-mouse IgG (whole-molecule)-peroxidase antibody (Sigma Aldrich, A9044) in 10 mL of TBS-T at RT for 1 h. Images were obtained at RT using chemiluminescent signals.

Liposome Cosedimentation Assay

The liposome cosedimentation experiments were performed as previously described, with slight modifications, by Zhu et al. (2014). Liposomes were prepared from 50% PC and 50% of the indicated lipids (PS, PE, or PI4P). The lipid mixtures (dissolved in chloroform) were dried by nitrogen gas, and

the dried lipid was resuspended in liposome buffer and sonicated for 20 min. For each protein, a final concentration of 2 μM, 3 μM, or 4 μM protein solution was incubated with or without 100 μg of lipid mixture at RT for 30 min. Then, the samples were centrifuged at 20,000*g* at 4°C for 30 min. Then, the pellets and supernatants were separated, subjected to SDS-PAGE, and stained with Coomassie Blue. The percentage of the bound proteins was analyzed by ImageJ software.

Statistical Analysis

Statistical analysis was performed via the SPSS software package (version 22.0; IBM). The data represent the means ± SDs based on three independent biological replicates. Two-tailed Student's *t* tests (*t* test) were performed to determine statistical significance, and the threshold was set at 0.05.

Accession Numbers

The sequence data from this article can be found in The Arabidopsis Information Resource (https://www.arabidopsis.org/) or GenBank (http://www.ncbi.nlm.nih.gov/genbank/) databases under the following accession numbers: At-*ALA3* (AT1G59820), At-*ALA1* (AT5G04930), At-*ALA2* (AT5G44240), At-*ALA4* (AT1G17500), At-*ALA5* (AT1G72700), At-*ALA6* (AT1G54280), At-*ALA7* (AT3G13900), At-*ALA8* (AT3G27870), At-*ALA9* (AT1G68710), At-*ALA10* (AT3G25610), At-*ALA11* (AT1G13210), At-*ALA12* (AT1G26130), At-*RabA4d* (AT3G12160), At-*RabA4b* (AT4G39990), At-*RabD1* (AT3G11730), At-*RabA1g* (AT3G15060), At-*VGD1* (AT2G47040), At-*ARA6* (AT3G54840), *MFGE8 (lactadherin)* (NM_176610), and At-*ROP6* (AT4G35020).

Supplemental Data

Supplemental Figure 1. The distribution pattern of the FM4-64-labeled compartment in *ala1*, *ala6*, *ala7*, *ala9*, and *ala12* mutant pollen tubes was comparable to that in Col-0 (supports Figure 1).

Supplemental Figure 2. The pollen tube growth of the *ala3* mutant is less sensitive to BFA than that of Col-0 (supports Figure 1).

Supplemental Figure 3. *ALA3* is abundantly expressed in inflorescences, mature pollen grains, and pollen tubes (supports Figure 2).

Supplemental Figure 4. Kymograph showing ALA3-GFP not colocalized with Golgi or LE (supports Figure 2).

Supplemental Figure 5. The exogenous inhibitors BFA, LatB, and Wort can significantly perturb the polar localization of ALA3-GFP in pollen tubes (supports Figure 2).

Supplemental Figure 6. ALA3-GFP colocalizes with RFP-RabA4b at the pollen tube tip (supports Figure 3).

Supplemental Figure 7. Kymograph showing EGFP-Lact-C2 colocalized or not colocalized with certain endomembrane compartments (supports Figure 4).

Supplemental Figure 8. The exogenous inhibitors BFA, LatB, and Wort can significantly perturb the polar localization of EGFP-Lact-C2 in pollen tubes (supports Figure 4).

Supplemental Figure 9. The distribution of the ER and Golgi is not affected by the *ala3* mutation (supports Figure 5).

Supplemental Figure 10. The velocities of the TGN/EE in Col-0 and *ala3* are comparable (supports Figure 5).

Supplemental Figure 11. Localization pattern of mCITRINE-Lact-C2 PS biosensor is similar to the EGFP-Lact-C2 PS biosensor in Col-0 and *ala3* (supports Discussion).

Supplemental Figure 12. The levels of internalized FM4-64 in Col-0 and *ala3* are similar (supports Discussion).

Supplemental Figure 13. Different forms of some Rab GTPases can directly bind to PS in vitro (supports Discussion).

Supplemental Figure 14. Different forms of RabA4d can directly bind to PS but not PE or PC in vitro (supports Discussion).

Supplemental Table. Primers used in this study.

Supplemental Movie 1. FM4-64 distributes in inverted-cone zone of the Col-0 pollen tube (supports Figure 1).

Supplemental Movie 2. YFP-RabA4b localizes inverted-cone zone of the Col-0 pollen tube (supports Figure 1).

Supplemental Movie 3. FM4-64 moved in a disordered manner of the subapical region of *ala3* mutant pollen tube (supports Figure 1).

Supplemental Movie 4. YFP-RabA4b moved in a disordered manner of the subapical region of *ala3* mutant pollen tube (supports Figure 1).

Supplemental Movie 5. ALA3-GFP signals were largely distributed in the apical and subapical regions of the pollen tube (supports Figure 2).

Supplemental Movie 6. RFP-RabA4d localizes inverted-cone zone of the Col-0 pollen tube (supports Figure 3).

Supplemental Movie 7. RFP-RabA4d moved in a disordered manner of the subapical region of *ala3* mutant pollen tube (supports Figure 3).

Supplemental Movie 8. EGFP-Lact-C2 PS biosensor was abundantly localized at the inverted-cone zone of Col-0 pollen tube (supports Figure 4).

Supplemental Movie 9. EGFP-Lact-C2 PS biosensor was abundantly localized at the inverted-cone zone of Col-0 pollen tube (supports Figure 4).

Supplemental Movie 10. EGFP-Lact-C2 PS biosensor moved in a disordered manner of the subapical region of *ala3* mutant pollen tube (supports Figure 4).

Supplemental Movie 11. VHAa1-RFP TGN/EE marker localizes at the shank region of Col-0 pollen tube (supports Figure 5).

Supplemental Movie 12. mCherry-VTI12 TGN/EE marker localizes at the apical, subapical, and shank regions of Col-0 pollen tube (supports Figure 5).

Supplemental Movie 13. VHAa1-RFP TGN/EE marker localizes at the shank region of *ala3* mutant pollen tube (supports Figure 5).

Supplemental Movie 14. mCherry-VTI12 TGN/EE marker was abundantly accumulate at the subapical region of *ala3* mutant pollen tube (supports Figure 5).

Supplemental Movie 15. mCherry-RabA1e RE marker localizes at the apical and shank region of Col-0 pollen tube (supports Figure 7).

Supplemental Movie 16. mCherry-RabA1g RE marker localizes at the apical and shank region of Col-0 pollen tube (Supports Figure 7).

Supplemental Movie 17. mCherry-RabA1e RE marker was abundantly accumulate at the subapical region of *ala3* mutant pollen tube (supports Figure 7).

Supplemental Movie 18. mCherry-RabA1g RE marker was abundantly accumulate at the subapical region of *ala3* mutant pollen tube (supports Figure 7).

ACKNOWLEDGMENTS

We thank Tonglin Mao (China Agricultural University), Xiangfeng Wang (China Agricultural University), and Ruixi Li (Southern University of Science and Technology) for valuable comments on the manuscript. We thank Lijia

Qu (Peking University), Genji Qin (Peking University), Yan Zhang (Shangdong Agricultural University), and Jianwei Pan (Lanzhou University) for sharing seeds. We thank the Core Facility of the School of Life Sciences, Lanzhou University, for technical assistance. This work was supported by the National Natural Science Foundation of China (grants 31722005, 31970195, and 31670180) and the Fundamental Research Funds for the Central Universities (grants lzujbky-2019-75 and lzujbky-2020-sp04).

AUTHOR CONTRIBUTIONS

Y.X. and Y.N. conceived the study and designed the research; Y.Z., Y.Y., D.Q., and T.T.F. performed the research; Y.Z., Y.Y., C.L., Y.S., S.L., and L.A. analyzed the data; Y.X., Y.N., Y.Z., and Y.Y. wrote the article.

Received October 28, 2019; revised July 17, 2020; accepted August 17, 2020; published August 18, 2020.

REFERENCES

Bhuin, T., and Roy, J.K. (2014). Rab proteins: The key regulators of intracellular vesicle transport. Exp. Cell Res. **328:** 1–19.

Bigay, J., and Antonny, B. (2012). Curvature, lipid packing, and electrostatics of membrane organelles: Defining cellular territories in determining specificity. Dev. Cell **23:** 886–895.

Botella, C., Sautron, E., Boudiere, L., Michaud, M., Dubots, E., Yamaryo-Botté, Y., Albrieux, C., Marechal, E., Block, M.A., and Jouhet, J. (2016). ALA10, a phospholipid flippase, controls FAD2/FAD3 desaturation of phosphatidylcholine in the ER and affects chloroplast lipid composition in *Arabidopsis thaliana*. Plant Physiol. **170:** 1300–1314.

Bottanelli, F., Foresti, O., Hanton, S., and Denecke, J. (2011). Vacuolar transport in tobacco leaf epidermis cells involves a single route for soluble cargo and multiple routes for membrane cargo. Plant Cell **23:** 3007–3025.

Caillaud, M.C. (2019). Anionic lipids: A pipeline connecting key players of plant cell division. Front Plant Sci **10:** 419.

Chebli, Y., Kroeger, J., and Geitmann, A. (2013). Transport logistics in pollen tubes. Mol. Plant **6:** 1037–1052.

Cheung, A.Y., and Wu, H.M. (2008). Structural and signaling networks for the polar cell growth machinery in pollen tubes. Annu. Rev. Plant Biol. **59:** 547–572.

de Graaf, B.H.J., Cheung, A.Y., Andreyeva, T., Levasseur, K., Kieliszewski, M., and Wu, H.M. (2005). Rab11 GTPase-regulated membrane trafficking is crucial for tip-focused pollen tube growth in tobacco. Plant Cell **17:** 2564–2579.

Dettmer, J., Hong-Hermesdorf, A., Stierhof, Y.D., and Schumacher, K. (2006). Vacuolar H^+-ATPase activity is required for endocytic and secretory trafficking in *Arabidopsis*. Plant Cell **18:** 715–730.

Ebine, K., Inoue, T., Ito, J., Ito, E., Uemura, T., Goh, T., Abe, H., Sato, K., Nakano, A., and Ueda, T. (2014). Plant vacuolar trafficking occurs through distinctly regulated pathways. Curr. Biol. **24:** 1375–1382.

Ellinger, D., Glöckner, A., Koch, J., Naumann, M., Stürtz, V., Schütt, K., Manisseri, C., Somerville, S.C., and Voigt, C.A. (2014). Interaction of the *Arabidopsis* GTPase RabA4c with its effector PMR4 results in complete penetration resistance to powdery mildew. Plant Cell **26:** 3185–3200.

Fabrice, T.N., Vogler, H., Draeger, C., Munglani, G., Gupta, S., Herger, A.G., Knox, P., Grossniklaus, U., and Ringli, C. (2018). LRX proteins play a crucial role in pollen grain and pollen tube cell wall development. Plant Physiol. **176:** 1981–1992.

Fu, Y., Wu, G., and Yang, Z. (2001). Rop GTPase-dependent dynamics of tip-localized F-actin controls tip growth in pollen tubes. J. Cell Biol. **152:** 1019–1032.

Geldner, N., Dénervaud-Tendon, V., Hyman, D.L., Mayer, U., Stierhof, Y.D., and Chory, J. (2009). Rapid, combinatorial analysis of membrane compartments in intact plants with a multicolor marker set. Plant J. **59:** 169–178.

Gibbon, B.C., Kovar, D.R., and Staiger, C.J. (1999). Latrunculin B has different effects on pollen germination and tube growth. Plant Cell **11:** 2349–2363.

Gomès, E., Jakobsen, M.K., Axelsen, K.B., Geisler, M., and Palmgren, M.G. (2000). Chilling tolerance in *Arabidopsis* involves ALA1, a member of a new family of putative aminophospholipid translocases. Plant Cell **12:** 2441–2454.

Grebnev, G., Ntefidou, M., and Kost, B. (2017). Secretion and endocytosis in pollen tubes: Models of tip growth in the spot light. Front Plant Sci **8:** 154.

Grosshans, B.L., Ortiz, D., and Novick, P. (2006). Rabs and their effectors: achieving specificity in membrane traffic. Proc. Natl. Acad. Sci. USA **103:** 11821–11827.

Guo, Z., Lu, J., Wang, X., Zhan, B., Li, W., and Ding, S.W. (2017). Lipid flippases promote antiviral silencing and the biogenesis of viral and host siRNAs in *Arabidopsis*. Proc. Natl. Acad. Sci. USA **114:** 1377–1382.

Hempel, F., Stenzel, I., Heilmann, M., Krishnamoorthy, P., Menzel, W., Golbik, R., Helm, S., Dobritzsch, D., Baginsky, S., Lee, J., Hoehenwarter, W., and Heilmann, I. (2017). MAPKs influence pollen tube growth by controlling the formation of phosphatidylinositol 4,5-bisphosphate in an apical plasma membrane domain. Plant Cell **29:** 3030–3050.

Hepler, P.K., Vidali, L., and Cheung, A.Y. (2001). Polarized cell growth in higher plants. Annu. Rev. Cell Dev. Biol. **17:** 159–187.

Jean, S., and Kiger, A.A. (2012). Coordination between RAB GTPase and phosphoinositide regulation and functions. Nat. Rev. Mol. Cell Biol. **13:** 463–470.

Jia, H., Li, J., Zhu, J., Fan, T., Qian, D., Zhou, Y., Wang, J., Ren, H., Xiang, Y., and An, L. (2013). *Arabidopsis* CROLIN1, a novel plant actin-binding protein, functions in cross-linking and stabilizing actin filaments. J. Biol. Chem. **288:** 32277–32288.

Johnson, M.A., Harper, J.F., and Palanivelu, R. (2019). A fruitful journey: Pollen tube navigation from germination to fertilization. Annu. Rev. Plant Biol. **70:** 809–837.

Kjos, I., Vestre, K., Guadagno, N.A., Borg Distefano, M., and Progida, C. (2018). Rab and Arf proteins at the crossroad between membrane transport and cytoskeleton dynamics. Biochim. Biophys. Acta Mol. Cell Res. **1865:** 1397–1409.

Kost, B., Lemichez, E., Spielhofer, P., Hong, Y., Tolias, K., Carpenter, C., and Chua, N.H. (1999). Rac homologues and compartmentalized phosphatidylinositol 4, 5-bisphosphate act in a common pathway to regulate polar pollen tube growth. J. Cell Biol. **145:** 317–330.

Kulakowski, G., Bousquet, H., Manneville, J.B., Bassereau, P., Goud, B., and Oesterlin, L.K. (2018). Lipid packing defects and membrane charge control RAB GTPase recruitment. Traffic **19:** 536–545.

López-Marqués, R.L., Poulsen, L.R., Hanisch, S., Meffert, K., Buch-Pedersen, M.J., Jakobsen, M.K., Pomorski, T.G., and Palmgren, M.G. (2010). Intracellular targeting signals and lipid specificity determinants of the ALA/ALIS P_4-ATPase complex reside in the catalytic ALA α-subunit. Mol. Biol. Cell **21:** 791–801.

Luo, N., Yan, A., Liu, G., Guo, J., Rong, D., Kanaoka, M.M., Xiao, Z., Xu, G., Higashiyama, T., Cui, X., and Yang, Z. (2017). Exocytosis-coordinated mechanisms for tip growth underlie pollen tube growth guidance. Nat. Commun. **8:** 1687.

Luu, D.T., Martinière, A., Sorieul, M., Runions, J., and Maurel, C. (2012). Fluorescence recovery after photobleaching reveals high cycling dynamics of plasma membrane aquaporins in *Arabidopsis* roots under salt stress. Plant J. **69:** 894–905.

Mazel, A., Leshem, Y., Tiwari, B.S., and Levine, A. (2004). Induction of salt and osmotic stress tolerance by overexpression of an intracellular vesicle trafficking protein AtRab7 (AtRabG3e). Plant Physiol. **134:** 118–128.

McDowell, S.C., López-Marqués, R.L., Poulsen, L.R., Palmgren, M.G., and Harper, J.F. (2013). Loss of the *Arabidopsis thaliana* P_4-ATPase ALA3 reduces adaptability to temperature stresses and impairs vegetative, pollen, and ovule development. PLoS One **8:** e62577.

Muthusamy, B.P., Natarajan, P., Zhou, X., and Graham, T.R. (2009). Linking phospholipid flippases to vesicle-mediated protein transport. Biochim. Biophys. Acta **1791:** 612–619.

Nielsen, E., Cheung, A.Y., and Ueda, T. (2008). The regulatory RAB and ARF GTPases for vesicular trafficking. Plant Physiol. **147:** 1516–1526.

Niu, Y., Qian, D., Liu, B., Ma, J., Wan, D., Wang, X., He, W., and Xiang, Y. (2017). ALA6, a P_4-type ATPase, is involved in heat stress responses in *Arabidopsis thaliana*. Front Plant Sci **8:** 1732.

Noack, L.C., and Jaillais, Y. (2017). Precision targeting by phosphoinositides: How PIs direct endomembrane trafficking in plants. Curr. Opin. Plant Biol. **40:** 22–33.

Peng, J., Ilarslan, H., Wurtele, E.S., and Bassham, D.C. (2011). AtRabD2b and AtRabD2c have overlapping functions in pollen development and pollen tube growth. BMC Plant Biol. **11:** 25.

Platre, M.P., et al. (2019). Developmental control of plant Rho GTPase nano-organization by the lipid phosphatidylserine. Science **364:** 57–62.

Platre, M.P., et al. (2018). A combinatorial lipid code shapes the electrostatic landscape of plant endomembranes. Dev. Cell **45:** 465–480.e11.

Potocký, M., Pleskot, R., Pejchar, P., Vitale, N., Kost, B., and Zárský, V. (2014). Live-cell imaging of phosphatidic acid dynamics in pollen tubes visualized by Spo20p-derived biosensor. New Phytol. **203:** 483–494.

Poulsen, L.R., López-Marqués, R.L., McDowell, S.C., Okkeri, J., Licht, D., Schulz, A., Pomorski, T., Harper, J.F., and Palmgren, M.G. (2008). The *Arabidopsis* P_4-ATPase ALA3 localizes to the golgi and requires a β-subunit to function in lipid translocation and secretory vesicle formation. Plant Cell **20:** 658–676.

Poulsen, L.R., López-Marqués, R.L., Pedas, P.R., McDowell, S.C., Brown, E., Kunze, R., Harper, J.F., Pomorski, T.G., and Palmgren, M. (2015). A phospholipid uptake system in the model plant *Arabidopsis thaliana*. Nat. Commun. **6:** 7649.

Preuss, M.L., Serna, J., Falbel, T.G., Bednarek, S.Y., and Nielsen, E. (2004). The *Arabidopsis* Rab GTPase RabA4b localizes to the tips of growing root hair cells. Plant Cell **16:** 1589–1603.

Qu, X., Zhang, H., Xie, Y., Wang, J., Chen, N., and Huang, S. (2013). *Arabidopsis* villins promote actin turnover at pollen tube tips and facilitate the construction of actin collars. Plant Cell **25:** 1803–1817.

Roland, B.P., and Graham, T.R. (2016). Decoding P_4-ATPase substrate interactions. Crit. Rev. Biochem. Mol. Biol. **51:** 513–527.

Rutherford, S., and Moore, I. (2002). The *Arabidopsis* Rab GTPase family: Another enigma variation. Curr. Opin. Plant Biol. **5:** 518–528.

Simon, M.L.A., Platre, M.P., Marquès-Bueno, M.M., Armengot, L., Stanislas, T., Bayle, V., Caillaud, M.C., and Jaillais, Y. (2016). A PtdIns(4)P-driven electrostatic field controls cell membrane identity and signalling in plants. Nat. Plants **2:** 16089.

Stenmark, H. (2009). Rab GTPases as coordinators of vesicle traffic. Nat. Rev. Mol. Cell Biol. **10:** 513–525.

Szumlanski, A.L., and Nielsen, E. (2009). The Rab GTPase RabA4d regulates pollen tube tip growth in *Arabidopsis thaliana*. Plant Cell **21:** 526–544.

Thole, J.M., Vermeer, J.E., Zhang, Y., Gadella, T.W., Jr., and Nielsen, E. (2008). *Root hair defective4* encodes a phosphatidylinositol-4-phosphate phosphatase required for proper root hair development in *Arabidopsis thaliana*. Plant Cell **20:** 381–395.

Thomas, L.L., van der Vegt, S.A., and Fromme, J.C. (2019). A steric gating mechanism dictates the substrate specificity of a Rab-GEF. Dev. Cell **48:** 100–114.e9.

Uemura, T., and Ueda, T. (2014). Plant vacuolar trafficking driven by RAB and SNARE proteins. Curr. Opin. Plant Biol. **22:** 116–121.

Underwood, W., Ryan, A., and Somerville, S.C. (2017). An *Arabidopsis* lipid flippase is required for timely recruitment of defenses to the host-pathogen interface at the plant cell surface. Mol. Plant **10:** 805–820.

Vermeer, J.E., van Leeuwen, W., Tobeña-Santamaria, R., Laxalt, A.M., Jones, D.R., Divecha, N., Gadella, T.W., Jr., and Munnik, T. (2006). Visualization of PtdIns3P dynamics in living plant cells. Plant J. **47:** 687–700.

Vernoud, V., Horton, A.C., Yang, Z., and Nielsen, E. (2003). Analysis of the small GTPase gene superfamily of *Arabidopsis*. Plant Physiol. **131:** 1191–1208.

Woollard, A.A., and Moore, I. (2008). The functions of Rab GTPases in plant membrane traffic. Curr. Opin. Plant Biol. **11:** 610–619.

Xiang, Y., Huang, X., Wang, T., Zhang, Y., Liu, Q., Hussey, P.J., and Ren, H. (2007). ACTIN BINDING PROTEIN 29 from *Lilium* pollen plays an important role in dynamic actin remodeling. Plant Cell **19:** 1930–1946.

Xu, P., Baldridge, R.D., Chi, R.J., Burd, C.G., and Graham, T.R. (2013). Phosphatidylserine flipping enhances membrane curvature and negative charge required for vesicular transport. J. Cell Biol. **202:** 875–886.

Yeung, T., Gilbert, G.E., Shi, J., Silvius, J., Kapus, A., and Grinstein, S. (2008). Membrane phosphatidylserine regulates surface charge and protein localization. Science **319:** 210–213.

Yin, C., Karim, S., Zhang, H., and Aronsson, H. (2017). *Arabidopsis* RabF1 (ARA6) is involved in salt stress and dark-Induced senescence (DIS). Int. J. Mol. Sci. **18:** 309.

Zerial, M., and McBride, H. (2001). Rab proteins as membrane organizers. Nat. Rev. Mol. Cell Biol. **2:** 107–117.

Zhang, X., et al. (2020). Arabidopsis flippases cooperate with ARF GTPase exchange factors to regulate the trafficking and polarity of PIN auxin transporters. Plant Cell **32:** 1644–1664.

Zhang, X., and Oppenheimer, D.G. (2009). IRREGULAR TRICHOME BRANCH 2 (ITB2) encodes a putative aminophospholipid translocase that regulates trichome branch elongation in *Arabidopsis*. Plant J. **60:** 195–206.

Zhang, Y., He, J., Lee, D., and McCormick, S. (2010). Interdependence of endomembrane trafficking and actin dynamics during polarized growth of *Arabidopsis* pollen tubes. Plant Physiol. **152:** 2200–2210.

Zhao, Y., Yan, A., Feijó, J.A., Furutani, M., Takenawa, T., Hwang, I., Fu, Y., and Yang, Z. (2010). Phosphoinositides regulate clathrin-dependent endocytosis at the tip of pollen tubes in *Arabidopsis* and tobacco. Plant Cell **22:** 4031–4044.

Zhu, J., Nan, Q., Qin, T., Qian, D., Mao, T., Yuan, S., Wu, X., Niu, Y., Bai, Q., An, L., and Xiang, Y. (2017). Higher-ordered actin structures remodeled by *Arabidopsis* ACTIN-DEPOLYMERIZING FACTOR5 are important for pollen germination and pollen tube growth. Mol. Plant **10:** 1065–1081.

Zhu, J., Wu, X., Yuan, S., Qian, D., Nan, Q., An, L., and Xiang, Y. (2014). Annexin5 plays a vital role in *Arabidopsis* pollen development via Ca^{2+}-dependent membrane trafficking. PLoS One **9:** e102407.